Published for SISSA by Springer

Received: April 5, 2024
Accepted: June 22, 2024
Published: July 11, 2024

Search for the $B_s^0 \to \mu^+\mu^-\gamma$ decay

The LHCb collaboration

E-mail: irene.bachiller@cern.ch

Abstract: A search for the fully reconstructed $B_s^0 \to \mu^+\mu^-\gamma$ decay is performed at the LHCb experiment using proton-proton collisions at $\sqrt{s} = 13\,\text{TeV}$ corresponding to an integrated luminosity of $5.4\,\text{fb}^{-1}$. No significant signal is found and upper limits on the branching fraction in intervals of the dimuon mass are set

$$\begin{aligned}
\mathcal{B}(B_s^0 \to \mu^+\mu^-\gamma) &< 4.2\times 10^{-8}, \quad m(\mu^+\mu^-) \in [2m_\mu,\ 1.70]\,\text{GeV}/c^2,\\
\mathcal{B}(B_s^0 \to \mu^+\mu^-\gamma) &< 7.7\times 10^{-8}, \quad m(\mu^+\mu^-) \in [1.70,\ 2.88]\,\text{GeV}/c^2,\\
\mathcal{B}(B_s^0 \to \mu^+\mu^-\gamma) &< 4.2\times 10^{-8}, \quad m(\mu^+\mu^-) \in [3.92,\ m_{B_s^0}]\,\text{GeV}/c^2,
\end{aligned}$$

at 95% confidence level. Additionally, upper limits are set on the branching fraction in the $[2m_\mu,\ 1.70]\,\text{GeV}/c^2$ dimuon mass region excluding the contribution from the intermediate $\phi(1020)$ meson, and in the region combining all dimuon-mass intervals.

Keywords: B Physics, Flavour Physics, Hadron-Hadron Scattering , Rare Decay

ArXiv ePrint: 2404.03375

https://doi.org/10.1007/JHEP07(2024)101

Contents

JHEP07(2024)101

1 Introduction

Rare decays of b hadrons involving flavour-changing neutral currents, such as those mediated by $b \to sll$ transitions, are forbidden at tree level in the Standard Model (SM) and are thus suppressed. As a consequence these decays are sensitive probes of potential contributions of beyond the SM (BSM) particles. Measurements of branching fractions and angular distributions can probe new physics scenarios arising above the weak scale, encoded in the Wilson coefficients [1] of the weak effective theory, which at present are showing some tensions with the SM [2].

In this context, the $B^0_s \to \mu^+\mu^-\gamma$ decay[1] has attracted both theoretical and experimental interest as a powerful probe for investigating the aforementioned deviations from the SM. Compared to its nonradiative counterpart that is sensitive to the $\mathcal{O}^{(\prime)}_{10}$ operators, the $B^0_s \to \mu^+\mu^-\gamma$ decay offers sensitivity to a wider set of operators [3–6], as shown in figure 1. Adding a photon to the dimuon final state lifts the chiral suppression factor present in the $B^0_s \to \mu^+\mu^-$ decay, enhancing the total branching fraction, compensating the addition of the QED vertex [7, 8]. However, this additional photon comes with the added challenge of the local form factors describing the $B^0_s \to \gamma$ transitions. At low dimuon mass squared, q^2, below the charmonium resonances, the decay is mostly sensitive to the electromagnetic-dipole operators $\mathcal{O}^{(\prime)}_7$. This kinematic region is especially interesting since different approaches to the calculation of the $B^0_s \to \gamma$ local form factor result in different estimates of the branching fraction. In the low-q^2 region, these calculations have been done with single-pole [9] and

[1]The inclusion of charge-conjugate processes is implied throughout the text.

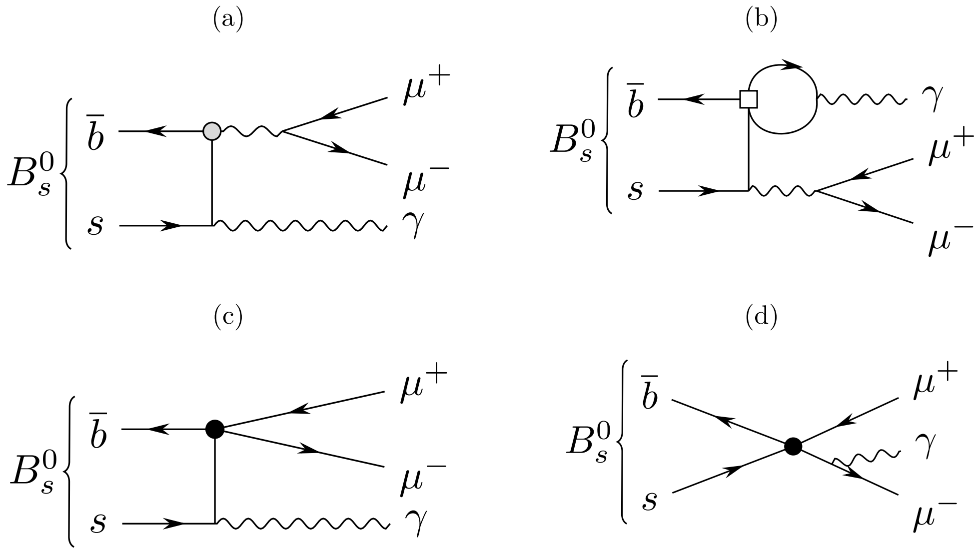

Figure 1. Diagrams contributing to $B_s^0 \to \mu^+\mu^-\gamma$ decay at lowest order. The grey circle denotes the electromagnetic-dipole operators $\mathcal{O}_7^{(\prime)}$. The empty square corresponds to any four-quark operator, where the quark-loop operators $\mathcal{O}_{1,2}$ dominate. The black circles denote the four-fermion operators $\mathcal{O}_{9,10}^{(\prime)}$.

multipole [10] parametrisations, soft-collinear effective theory (SCET) [11], and using the light-cone sum rules (LCSR) approach [12]. Above the $\psi(2S)$ resonance, this decay is sensitive to vector and axial-vector interactions dominated by the $\mathcal{O}_{9,10}^{(\prime)}$ operators. In this high-q^2 region, the form factors are calculated with lattice QCD (LQCD), making use of heavy quark effective theory (HQET) extrapolation [13] and assuming vector meson dominance (VMD) [14, 15]. Finally, at very high q^2 ($q^2 \gtrsim 25\,\text{GeV}^2/c^4$), this decay is dominated by final state radiation (FSR). This variety of contributions shapes the $B_s^0 \to \mu^+\mu^-\gamma$ q^2 spectrum for a photon energy larger than $50\,\text{MeV}/c^2$ [3, 16] as illustrated in figure 2. From ref. [9], the SM predictions of the branching fractions are $\mathcal{B}(B_s^0 \to \mu^+\mu^-\gamma)_{\text{low-}q^2} = (8.3 \pm 1.3) \times 10^{-9}$ and $\mathcal{B}(B_s^0 \to \mu^+\mu^-\gamma)_{\text{high-}q^2} = (8.9 \pm 1.0) \times 10^{-10}$, where low- and high-$q^2$ regions are respectively defined by $q^2 \in [0.04, 8.64]\,\text{GeV}^2/c^4$ and $q^2 \in [15.84, 28.27]\,\text{GeV}^2/c^4$.

The BaBar collaboration published a first search for the $B^0 \to \mu^+\mu^-\gamma$ decay, resulting in an upper limit of $\mathcal{B}(B^0 \to \mu^+\mu^-\gamma) < 1.6 \times 10^{-7}$ at 90% C.L [17], while the B_s^0 counterpart was not explored. At LHCb, the $B_s^0 \to \mu^+\mu^-\gamma$ decay was probed as a partially reconstructed background of the $B_s^0 \to \mu^+\mu^-$ decay, and a first upper limit was set on the branching fraction: $\mathcal{B}(B_s^0 \to \mu^+\mu^-\gamma) < 2.0 \times 10^{-9}$ at 95% C.L [18]. This result is limited to the high-q^2 region, due to the restricted dimuon mass search window of $[4.9\,\text{GeV}/c^2, m_{B_s^0}]$. To be sensitive to the low-q^2 range, and therefore to a richer set of Wilson coefficients, the full final state reconstruction is needed.

This paper presents the first search for the $B_s^0 \to \mu^+\mu^-\gamma$ decay with full final state reconstruction, and the first search for this decay at low q^2. Results are based on data collected with the LHCb detector in the years 2016–2018, corresponding to an integrated luminosity of $5.4\,\text{fb}^{-1}$ of proton-proton (pp) collisions at a centre-of-mass energy $\sqrt{s} = 13\,\text{TeV}$.

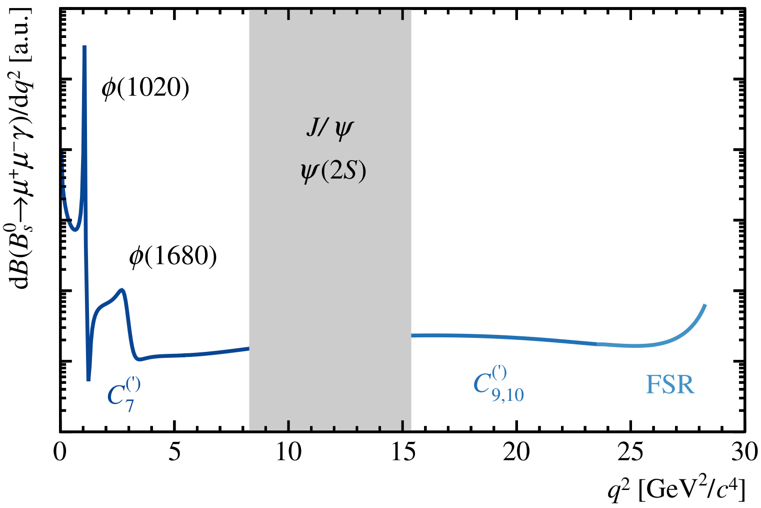

Figure 2. Illustration of the q^2 spectrum in $B_s^0 \to \mu^+\mu^-\gamma$ decays from refs. [3, 16] for a photon energy larger than $50\,\mathrm{MeV}/c^2$. The grey band corresponds to the excluded region dominated by $B_s^0 \to J/\psi\gamma$ and $B_s^0 \to \psi(2S)\gamma$ decays. The Wilson coefficients and the FSR are highlighted in the region of the spectrum where they are dominant. The magnitudes are chosen for illustrative purposes.

q^2 bin	I	II	III
q^2 [GeV^2/c^4]	$[4m_\mu^2, 2.89]$	$[2.89, 8.29]$	$[15.37, m_{B_s^0}^2]$
$m(\mu^+\mu^-)$ [GeV/c^2]	$[2m_\mu, 1.70]$	$[1.70, 2.88]$	$[3.92, m_{B_s^0}]$
$10^{10} \times \mathcal{B}(B_s^0 \to \mu^+\mu^-\gamma)$	82 ± 15	2.54 ± 0.34	9.1 ± 1.1
Fraction of $B_s^0 \to \mu^+\mu^-\gamma$	87%	2.7%	9.8%

Table 1. Mass range definition, predicted branching fraction, and the expected fraction of signal yield in the different q^2 bins as calculated in ref. [9].

2 Analysis strategy

The analysis is performed in the full kinematically accessible dimuon mass range, from the mass of the two muons, $2m_\mu$, up to the B_s^0 mass, $m_{B_s^0}$. The analysis is performed in three dimuon mass bins as defined in table 1. The value of $1.70\,\mathrm{GeV}/c^2$ is chosen to be above the region where the $\phi(1020)$,[2] and $\phi(1680)$ resonances contribute. Using the SM prediction of the differential branching fraction derived in ref. [9], the fraction of signal yield in each bin can be computed and is given in table 1.

Since bin I is dominated by the ϕ resonance, a complementary study is done in bin I excluding the ϕ mass region. This ϕ veto removes candidates with $m(\mu^+\mu^-) \in [989.6, 1073.4]\,\mathrm{MeV}/c^2$, as suggested in ref. [19]. The same selection optimisation and background modeling of bin I are used for bin I with the ϕ veto.

The signature of the $B_s^0 \to \mu^+\mu^-\gamma$ decay is two muons and one photon, with a combined invariant mass in the B_s^0 mass region and a decay vertex displaced with respect to the pp interaction vertex. This signature is exploited by the selection process, as described in

[2] Referred to as ϕ throughout the text.

JHEP07(2024)101

section 4. It includes the description of the trigger, preselection, and the two multivariate classifiers based on a multilayer perceptron (MLP) [20] implemented in the TMVA toolkit [21], applied to reduce the backgrounds. The $B_s^0 \to \phi\gamma$ decay, with $\phi \to K^+K^-$, is used as control channel to assess the agreement of data and simulation as described in section 4.1.

The branching fraction of the signal is normalised to a well-known decay: $B_s^0 \to J/\psi\eta$, with $J/\psi \to \mu^+\mu^-$ and $\eta \to \gamma\gamma$ as presented in section 5. The signal yields are estimated using an extended unbinned maximum-likelihood fit to the final-state mass distribution, where the signal and background are modelled as described in section 5.2. Finally the results are presented in section 6.

To avoid experimenter's bias, the candidates in the signal region, $m(\mu^+\mu^-\gamma) \in [5.25, 5.55]$ GeV/c^2, were not examined until the selection and analysis procedures were finalised. Most of the studies are done separately per data-taking year to account for possible variations in data-taking conditions, and merged at the last step of the analysis.

3 Detector and simulation

The LHCb detector [22, 23] is a single-arm forward spectrometer covering the pseudorapidity range $2 < \eta < 5$, designed for the study of particles containing b or c quarks. The detector includes a high-precision tracking system consisting of a silicon-strip vertex detector surrounding the pp interaction region [24], a large-area silicon-strip detector located upstream of a dipole magnet with a bending power of about 4 Tm, and three stations of silicon-strip detectors and straw drift tubes [25] placed downstream of the magnet.

The tracking system provides a measurement of the momentum, p, of charged particles with a relative uncertainty that varies from 0.5% at low momentum to 1.0% at 200 GeV/c. The minimum distance of a track to a primary pp collision vertex (PV), the impact parameter (IP), is measured with a resolution of $(15 + 29/p_{\mathrm{T}})\,\mu\mathrm{m}$ [24], where p_{T} is the component of the momentum transverse to the beam, in GeV/c. Different types of charged hadrons are distinguished using information from two ring-imaging Cherenkov detectors [26]. Photons, electrons and hadrons are identified by a calorimeter system consisting of scintillating-pad (SPD) and preshower detectors (PRS), an electromagnetic (ECAL) and a hadronic (HCAL) calorimeter. Muons are identified by a system composed of alternating layers of iron and multiwire proportional chambers [27].

The online event selection is performed by a trigger [28], which consists of a hardware stage, based on information from the calorimeter and muon systems, followed by a software stage, which applies a full event reconstruction.

Simulation is used to optimise the selection strategy, to estimate the background and signal shapes, and to calculate the efficiencies. The pp collisions are generated using Pythia [29, 30] with a specific LHCb configuration [31]. Decays of unstable particles are described by EvtGen [32], in which final-state radiation is generated using Photos [33]. The interaction of the generated particles with the detector, and its response, are implemented using the Geant4 toolkit [34, 35] as described in ref. [36]. The theory model for the signal simulation is computed in ref. [16].

In simulation, the same reconstruction algorithms as in data are applied. Background candidates can contaminate the simulated samples if they are incorrectly reconstructed. A

JHEP07(2024)101

truth-matching algorithm is used to match reconstructed candidates with generated candidates. The algorithm matches the reconstructed objects with the generator level information for the final state particles and the particles in the decay chain.

4 Selection

Signal candidates are first selected by the hardware trigger, which requires candidates with either one muon with high transverse momentum, or one photon with high transverse momentum. Subsequently, the two-stage software trigger imposes requirements on the muon transverse momentum and track reconstruction quality. To maximise the signal selection efficiency, candidates triggered by particles not associated with the signal candidates are also retained for further analysis, increasing the number of candidates by 10%. A multivariate classifier based on topological criteria complements the software trigger selection [37]. The same hardware and first-stage software trigger is used for the normalisation channel, the $B_s^0 \to J/\psi\eta$ decay. A second-stage software trigger that selects candidates with two reconstructed muons with invariant mass in the J/ψ mass region is used for the normalization channel. The trigger for the control channel, $B_s^0 \to \phi\gamma$, is chosen to select candidates with one photon and two charged tracks with reconstructed invariant mass in the ϕ mass region.

A preselection is applied to the $B_s^0 \to \mu^+\mu^-\gamma$ candidates. The photon must have a transverse momentum larger than 1000 MeV/c. In order to separate photon clusters from non-electromagnetic charged clusters, a neural network classifier is employed [38]. The input variables of this neural network are related to the energy deposits in each calorimeter and the shape of the cluster. The muons must have a transverse momentum larger than 250 MeV/c and good track reconstruction quality. To avoid contributions from charmonia, candidates with a dimuon mass in the range $[2.88, 3.92]$ GeV/c^2 are rejected. The B_s^0 candidate must have a transverse momentum larger than 500 MeV/c and a good quality decay vertex.

The preselection requirements on the normalisation channel are the same to that of the signal. Additional requirements on the $B_s^0 \to J/\psi\eta$ candidates are that the two photons (muons) from the η (J/ψ) decay must have an invariant mass within 105 MeV/c^2 (100 MeV/c^2) of the known η (J/ψ) mass [39].

The candidates of the control channel are selected with the same requirements on the kinematic variables as the signal channel with some additional requirements to select $B_s^0 \to \phi\gamma$ candidates. The photon transverse momentum must be larger than 2.5 GeV/c and the invariant mass of the two kaons should be within 15 MeV/c^2 of the known ϕ mass [39].

Further requirements on the particle identification (PID) information of the two muons are imposed in order to reject misidentified hadronic background. The muon identification (charged PID) uses multivariate techniques to combine information from different subsystems taking correlations into account [40]. The same muon identification requirement is applied to the signal and normalisation channels, while in the control channel, a different charged PID requirement is designed to select kaon tracks.

A further selection is applied to reject photons from $\pi^0 \to \gamma\gamma$ decays where they are reconstructed as a single cluster due to the limited calorimeter granularity, referred to as merged. This photon identification is referred to as neutral PID. The neutral PID variable is the output of a multivariate classifier that is trained based on the shape of the electromagnetic

JHEP07(2024)101

cluster in the ECAL, the PRS and the SPD, for photons with transverse momentum larger than 2 GeV/c. Photons with lower transverse momentum cannot be mistaken for merged neutral pions [41], and are therefore not subject to the neutral PID requirements. The same photon identification requirements are applied to the signal, normalisation and control channels.

The sample of selected candidates is dominated by random combinations of muons and photons from other b-hadron decays in the same event, referred to as combinatorial background. To reduce this combinatorial contribution, candidates are rejected using a requirement on the response of an MLP classifier [42–44]. This classifier is trained using data outside the signal mass region defined in section 2 and simulated signal candidates weighted by the method explained in section 4.1. The variables used in the training are: the B_s^0 candidate vertex fit χ^2, the candidate IP, and the IP significance; the cosine of the angle between the momentum vector of the B_s^0 candidate and the line joining the PV and its decay vertex, referred to as the direction angle; the minimum distance between the two muon tracks; the minimum IP of the muons with respect to any PV; the energy and transverse momentum of the photon; the number of reconstructed π^0 and η mesons in the events that share a photon with the signal candidate; and the smallest mass difference between these π^0 and η candidates and their known masses.

The performance of the MLP classifier is evaluated using the Punzi figure of merit (FoM) [45]

$$\mathrm{FoM} = \frac{\epsilon_{\mathrm{sig}}}{\sigma/2 + \sqrt{N_{\mathrm{bkg}}}}\,, \tag{4.1}$$

where ϵ_{sig} is the signal efficiency, $\sigma = 5$ is the target statistical significance, and N_{bkg} is the number of background candidates expected in the signal region. The requirement on the MLP classifier is chosen to maximise the FoM of the signal, and the same requirement is applied to the control and normalisation channels.

To further reduce the remaining background, candidates are selected by a second MLP classifier. It is trained separately on each q^2 region using simulated data as signal proxy and data outside the signal regions as background proxy. This second MLP classifier takes as input: the cosine of the angle between the momentum of the positive charged muon in the B_s^0 candidate rest frame and the vector perpendicular to the plane defined by the B_s^0 momentum and the beam axis; the B_s^0 candidate's direction angle, its IP significance and its transverse momentum; the distance between the two muons in the $\eta - \phi$ plane;[3] the photon transverse momentum, energy and isolation; the muon smallest impact parameter significance, and the muon isolation.

The photon and muon isolation variables, quantify the probability that other tracks in the event originate from the same hadron decay as the signal candidates.

The photon isolation, $\mathrm{I}(\gamma)$, is defined as

$$\mathrm{I}(\gamma) \equiv \frac{p_{\mathrm{T}}(\gamma)}{p_{\mathrm{T}}(\gamma) + \sum\limits_{\mathrm{tracks}} p_{\mathrm{T}}(\mathrm{track})}, \tag{4.2}$$

[3]The symbols η and ϕ here refer to the pseudorapidity and azimuthal angle (in radians).

JHEP07(2024)101

where the sum in the denominator runs over all tracks within a cone of $\sqrt{\Delta\phi^2 + \Delta\eta^2} = 1$ around the photon direction. Similar variables were used in previous measurements of radiative decays by LHCb, as described in refs. [46, 47].

Two isolation variables are designed to quantify the muon isolation, each considering a different type of track: tracks that have been reconstructed both before and after the magnet (long tracks) and tracks reconstructed only in the vertex detector (VELO tracks), as defined in ref. [18].

The performance of the second MLP is also evaluated using the FoM from eq. (4.1). The optimal MLP requirement is chosen to maximise the FoM of the signal individually in each q^2 region. A loose MLP requirement is applied to the normalization channel in order to keep a large sample of normalization channel candidates.

4.1 Control channel

Since the signal simulation does not reproduce the distributions in data perfectly, the change in efficiency due to the discrepancies needs to be estimated. The agreement between data and simulation is studied by comparing background-subtracted data and simulation distributions in the control and normalisation channels with a twofold strategy. In a first step, weights are computed as the ratio of data and simulation in the control channel, and they are applied to the simulated samples. Then, the remaining discrepancies are measured on both the control and the normalisation channels.

As the reconstructed muon and photon distributions in the normalisation channel are different to those in the signal channel, a 3-body decay is used as control channel to correct the simulation. The $B_s^0 \to \phi\gamma$ decay, where the ϕ decays into K^+K^-, is therefore used to control the reconstructed variables such as isolation, vertex χ^2 and muon and photon kinematic distributions. The branching fraction of this decay, $(3.4 \pm 0.4) \times 10^{-5}$ [39], is more than three orders of magnitude larger than that of the signal, ensuring a large sample size to perform the comparisons.

The B_s^0 candidate mass distribution is fitted with a double-sided Crystal Ball (DSCB) function [48], comprising a Gaussian core with asymmetric tails, with the tail parameters fixed to values obtained from simulation. Partially reconstructed backgrounds, such as the $B \to \phi\gamma K$ decay, are described by an Argus function [49] convolved with a Gaussian function. The combinatorial background contribution is modelled by an exponential function. The resulting fit to the invariant-mass distribution of the $K^+K^-\gamma$ candidates, is shown in figure 3. The fitted $B_s^0 \to \phi\gamma$ yield is 36400 ± 400, where the uncertainty is statistical.

Background-subtracted distributions of variables are extracted using the *sPlot* method [50] and compared with simulation. To avoid large weights from candidates coming from the tails of the signal distribution, where the ratio between background and signal is large, the mass window $[5.0, 5.7]\,\text{GeV}/c^2$ is used.

To find the optimal binning of the control variables, the *GradBoost* weighting method [51] is used. To avoid a training bias, the control sample is randomly split into two parts and classifiers are trained on one part and tested on the other. The weight is obtained as the average of the output of the two classifiers.

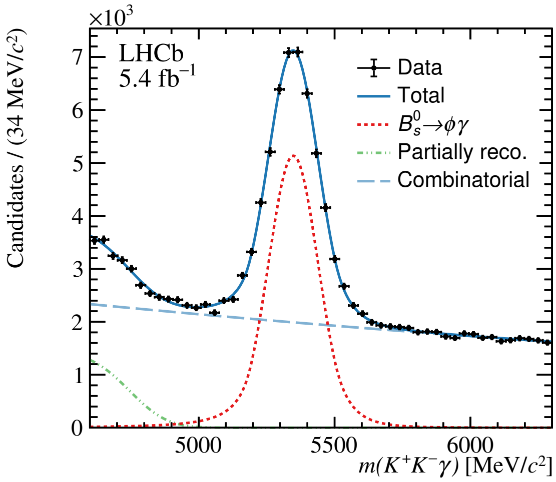

Figure 3. Mass distribution of $B_s^0 \to \phi\gamma$ candidates from data, used as control channel. The fit to the distribution is superimposed.

The weighting of the simulated samples is performed on three variables: the number of long tracks, the energy of the B_s^0 candidate, and its pseudorapidity. Weighting on the number of long tracks allows the correction of the variables related to the event occupancy such as isolation and vertex χ^2. Correcting for the discrepancies in energy and pseudorapidity of the B_s^0 candidates, results in better matching of the kinematic variables of the decay products.

After the weighting procedure, the remaining discrepancies between data and simulation in the variables used to train the MLP are calculated as the difference of the mean of the distributions and they range [1.4‰, 13%]. These discrepancies are propagated through the second MLP classifier by shifting each input variables by its maximum discrepancy value. The change of efficiency of the shifted MLP with respect to the central one is considered as a systematic uncertainty. This is the dominant source of uncertainty, being 40% of the total systematic uncertainty.

5 Branching fraction determination

The branching fraction of the signal is estimated by comparing its yield with a normalisation channel with well-known branching fractions: $B_s^0 \to J/\psi\eta$, with $J/\psi \to \mu^+\mu^-$ and $\eta \to \gamma\gamma$. This also allows a partial cancellation in the ratio of efficiencies which reduces the total uncertainty on the final result. The branching fraction is therefore expressed as

$$\mathcal{B}(B_s^0 \to \mu^+\mu^-\gamma) = \frac{\mathcal{B}_{\text{norm}}}{N_{\text{norm}}} \times \frac{\epsilon_{\text{norm}}}{\epsilon_{\text{sig}}} \times N_{\text{sig}}\,, \tag{5.1}$$

where ϵ_{norm} and ϵ_{sig} are the normalization and signal efficiencies, respectively. From the latest *CP*-averaged values of $\mathcal{B}(B_s^0 \to J/\psi\eta)$, $\mathcal{B}(J/\psi \to \mu^+\mu^-)$, and $\mathcal{B}(\eta \to \gamma\gamma)$, the combined branching fraction of the normalisation channel is $\mathcal{B}_{\text{norm}} = (9.3 \pm 1.6) \times 10^{-6}$ [39].

In order to estimate the $B_s^0 \to J/\psi\eta$ yield, a fit to the data is performed accounting for contributions from $B^0 \to J/\psi\eta$ decays and combinatorial background. The $B_s^0 \to J/\psi\eta$ candidates are modelled with a DSCB distribution with tail parameters fixed to values

JHEP07(2024)101

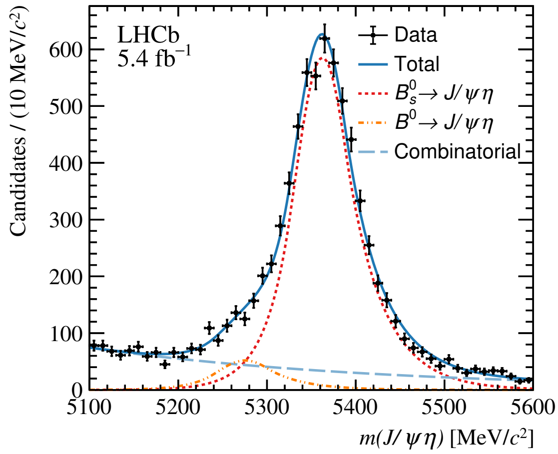

Figure 4. Mass distribution of $B_s^0 \to J/\psi\eta$ candidates from data, used as normalisation channel. The fit to the distribution is superimposed.

determined from simulation. The $B^0 \to J/\psi\eta$ contribution is modelled with the same shape used for the signal, with the mean shifted by the difference between the known B^0 and B_s^0 masses, and the relative contribution left floating to account for the difference in efficiency. The combinatorial background is modelled with an exponential distribution with the slope parameter left floating. The invariant-mass distribution for the selected candidates of the normalisation channel, and the fit result, are shown in figure 4. The fitted $B_s^0 \to J/\psi\eta$ yield is $N_{\text{norm}} = 5680 \pm 110$, where the uncertainty is statistical.

5.1 Efficiencies and their systematic uncertainties

The efficiencies to detect the signal and normalisation channels can be factorised as

$$\epsilon = \epsilon_{\text{Acceptance}} \times \epsilon_{\text{Preselection}} \times \epsilon_{\mu\text{PID}} \times \epsilon_{\gamma\text{PID}} \times \epsilon_{\text{Trigger}} \times \epsilon_{\text{MLP}}. \tag{5.2}$$

Each efficiency and its associated systematic uncertainty are evaluated relative to the preceding stage for the signal and normalisation channels. The acceptance efficiency is defined as the fraction of decays with daughters inside the detector acceptance.

The efficiency of the preselection described in section 4 includes the efficiency of reconstructing all the final state particles. It is calculated from simulation for both signal and normalisation channels. A systematic uncertainty associated with the truth-matching algorithm described in section 3 is estimated by fitting the reconstructed B_s^0 mass distribution of simulated candidates failing this algorithm.

The muon identification efficiency, $\epsilon_{\mu\text{PID}}$, is measured using high-purity calibration samples of $J/\psi \to \mu^+\mu^-$ decays, selected using only kinematic requirements [52]. The muon PID efficiency is evaluated as a function of the muon momentum and pseudorapidity, as well as the track multiplicity of the event using a dedicated procedure [52]. The resulting efficiency maps are applied to simulated samples to determine the integrated efficiency for the signal and normalisation channels. This method introduces two systematic uncertainties. The first one is associated to the background subtraction method used in the calibration samples and the second one from modeling the dependencies of the muon PID efficiency maps. These uncertainties are calculated for each data-taking year and they are in the range [6, 7]‰.

JHEP07(2024)101

The photon identification efficiency, $\epsilon_{\gamma\text{PID}}$, is estimated from data with a similar method as the one applied to muons. The efficiency is extracted from a sample of $\eta \to \mu^+\mu^-\gamma$ decays, as a function of photon momentum, pseudorapidity and number of tracks in the event. The integrated efficiency is computed using the corrected signal kinematics for signal and normalisation channels. Similarly to the charged PID method, this method introduces two systematic uncertainties in the signal to normalisation efficiency ratio. The first is associated to the fit and the background subtraction method in the $\eta \to \mu^+\mu^-\gamma$ decay. The second uncertainty is estimated from the modeling of the efficiency dependency. These uncertainties are calculated for each data-taking year and are in the range [1, 5]%.

The trigger efficiency, $\epsilon_{\text{Trigger}}$, is determined from data with the TISTOS method [53]. Trigger information is associated to the reconstructed candidates during the offline processing. A reconstructed signal candidate can be classified into three categories: candidates triggered on signal (TOS), triggered on parts of the underlying event that are independent of the tracks forming the signal candidate (TIS), or triggered on both elements of the signal candidate and the underlying event. The trigger efficiency can be estimated by exploiting the overlap between the TIS and TOS categories (TIS&TOS) and assuming that the signal decays are uncorrelated with the rest of the event. The trigger efficiency of a given decay channel, is computed from the number of triggered candidates, N_{Trigger}, with respect to a total of N_{Total} candidates as

$$\epsilon_{\text{Trigger}} = \frac{N_{\text{Trigger}}}{N_{\text{Total}}} = \frac{N_{\text{Trigger}}}{N_{\text{TIS}}} \times \epsilon_{\text{TIS}} = \frac{N_{\text{Trigger}}}{N_{\text{TIS}}} \frac{N_{\text{TIS\&TOS}}}{N_{\text{TOS}}}, \tag{5.3}$$

where N_i is the number of background-subtracted candidates triggered within the category i. The $B^0_s \to \phi\gamma$ candidates are used to calculate photon trigger efficiencies, while muon and TIS trigger efficiencies are calculated from $B^+ \to J/\psi K^+$ candidates. The signal trigger efficiencies are calculated by convolving the simulated signal kinematics on the following variables: $p_z(B)$ and $p_{\text{T}}(B)$ for TIS trigger, $p_{\text{T}}(\mu)$ and $\text{IP}(\mu)$ for the muon triggers, and $p_{\text{T}}(\gamma)$ for photon triggers. The systematic uncertainties of the trigger efficiencies are estimated by determining them with a different method that makes use of simulation. The efficiency ratios differ between the two methods by [2, 3]%, which is assigned as systematic uncertainty.

Finally, the efficiency of the first and second MLP requirements, ϵ_{MLP}, as well as their associated systematic uncertainties, are calculated for the signal and normalisation channels using the kinematically weighted simulation presented in section 4.1.

The ratio of efficiencies for each q^2 region and the single-event sensitivity, α, defined as

$$\alpha \equiv \frac{\mathcal{B}_{\text{norm}}}{N_{\text{norm}}} \times \frac{\epsilon_{\text{norm}}}{\epsilon_{\text{sig}}}, \tag{5.4}$$

are shown in table 2, for each q^2 bin.

5.2 Signal and background model

The signal yield is determined from fits to the invariant-mass distribution of the selected candidates. The signal model is extracted from simulation, and described with a DSCB function.

The background contamination can be divided into four categories: combinatorial background, partially reconstructed decays, peaking and misidentified backgrounds. Combinatorial

q^2 bin	I	II	III
$\epsilon_{\rm norm}/\epsilon_{\rm sig}$	0.85 ± 0.07	0.95 ± 0.08	2.20 ± 0.07
$\alpha[10^{-9}]$	1.40 ± 0.27	1.56 ± 0.30	3.60 ± 0.63

Table 2. Efficiency ratios and single-event sensitivities, for each q^2 bin. The uncertainties on the efficiency ratios include the systematic uncertainties presented in section 5.1. The uncertainties on α are the propagated uncertainties from $\mathcal{B}_{\rm norm}$, $N_{\rm norm}$ and $\epsilon_{\rm norm}/\epsilon_{\rm sig}$.

background candidates are distributed across the entire mass search region, peaking background candidates have a reconstructed mass close to the B_s^0 mass value, while partially reconstructed, and misidentified contributions populate the region below the B_s^0 mass.

The combinatorial background is modelled using an exponential function with the slope and yield parameters left free to float in the fit. Processes where one particle of the final state is not reconstructed, referred to as partially reconstructed background, contribute with a broad peak below the B_s^0 mass. Three decays are studied in simulation: $B_s^0 \to \mu^+\mu^-\phi$ with $\phi \to \pi^+\pi^-\pi^0$, $B^0 \to \mu^+\mu^-\eta'$ with $\eta' \to \rho^0\gamma$, and $B^0 \to D^-\mu^+\nu_\mu$ with $D^- \to \pi^0\mu^-\overline{\nu}_\mu$. The invariant-mass distributions of these three decays are fitted with Argus functions. To account for the energy resolution, the Argus distribution is convolved with a Gaussian function centered at zero. Since the value of the Argus cutoff parameter has to be consistent among the three q^2 bins, it is fixed to the average of the fitted values from simulation, on each decay and each q^2 region. The impact of fixing this parameter is evaluated using simulated pseudoexperiments, by comparing the baseline result with alternative fits in which the different cutoff parameters are fixed to the individual values or a single cutoff parameter is allowed to float. The difference in the fitted signal yield is considered as systematic uncertainty. The yield and other model parameters are left floating in the fit.

The main background processes contributing to the signal mass region, referred to as peaking backgrounds, are the $B^0 \to \mu^+\mu^-\pi^0$ decay with $\pi^0 \to \gamma\gamma$ and the $B^0_{(s)} \to \mu^+\mu^-\eta$ decay with $\eta \to \gamma\gamma$. These decays contribute to the background if one photon is not reconstructed or if both photons are reconstructed in the same calorimeter cluster. The mass distributions of these decays are extracted from simulation, and the shape parameters are fixed in the final mass fit. The $B^0 \to \mu^+\mu^-\pi^0$ decay is modelled by a DSCB function while the $B^0_{(s)} \to \mu^+\mu^-\eta$ is found to be well described by an Argus shape convolved with a Gaussian function. Their yields are estimated from the expected branching fractions in ref. [39], and the efficiencies determined from simulation. In the final mass fit, the yield parameters are Gaussian-constrained to the estimated values.

Apart from a slightly smaller mass and the CKM suppression, $B^0 \to \mu^+\mu^-\gamma$ decays differ from their B_s^0 counterpart by their light meson resonances. As discussed in ref. [16], $B^0 \to \gamma$ transition form factors involve the ρ and the ω resonances, while $B_s^0 \to \gamma$ transition form factors involve the ϕ resonance, all of them in the low-q^2 region (bin I) [39]. Assuming that the branching fraction in bin I is dominated by these resonances, one can approximate the number of candidates under the narrow-width approximation [9, 39]

$$\left.\frac{N_{B^0\to\mu^+\mu^-\gamma}}{N_{B_s^0\to\mu^+\mu^-\gamma}}\right|_{\rm I} \approx \frac{f_d}{f_s}\,\frac{\mathcal{B}(B^0\to\rho\gamma)\mathcal{B}(\rho\to\mu^+\mu^-)+\mathcal{B}(B^0\to\omega\gamma)\mathcal{B}(\omega\to\mu^+\mu^-)}{\mathcal{B}(B_s^0\to\phi\gamma)\mathcal{B}(\phi\to\mu^+\mu^-)} \approx 0.03,$$

where f_d and f_s are the fragmentation fractions [39]. In the two other q^2 regions, II and III, where there are not resonant contributions, the relative contribution of B^0 with respect to B_s^0 can be estimated as

$$\left.\frac{N_{B^0\to\mu^+\mu^-\gamma}}{N_{B_s^0\to\mu^+\mu^-\gamma}}\right|_{\mathrm{II}} \approx \left.\frac{N_{B^0\to\mu^+\mu^-\gamma}}{N_{B_s^0\to\mu^+\mu^-\gamma}}\right|_{\mathrm{III}} \approx \frac{f_d}{f_s}\left|\frac{V_{td}}{V_{ts}}\right|^2 \approx 0.17\,,$$

where V_{td} and V_{ts} are the CKM matrix elements. The $B^0\to\mu^+\mu^-\gamma$ contribution is therefore considered negligible within the signal statistical uncertainty in all the q^2 regions.

Physical backgrounds can also emerge from doubly misidentified hadronic decays. The main ones are $B_s^0\to\phi\gamma$ decays where $\phi\to K^+K^-$ and $B^0\to K^{*0}\gamma$ decays where $K^{*0}\to K^+\pi^-$. The mis-identification probabilities are determined as a function of the track momentum and transverse momentum, using $D^{*+}\to D^0\pi^+$ decays with $D^0\to K^-\pi^+$ with the method described in ref. [18], and their contributions are found to be negligible. The effect of neglecting these two contributions and the $B^0\to\mu^+\mu^-\gamma$ contamination is studied. The $\mathrm{CL_S}$ [54] method is applied to determine branching fraction limits from simulated pseudoexperiments generated from the mass sidebands under the background-only hypothesis, with and without including the three backgrounds in the fit. The two results differ by less than one percent, confirming that their contributions are negligible.

Other possible backgrounds were studied and found to be negligible, such as Λ_b decays, charmonium resonances decaying to muons and $B^0\to\pi^+\pi^-\pi^0$ decays with double pion misidentification and a merged π^0.

The possibility of contamination from the $B^{*0}\to B^0\gamma$ decay with $B^0\to\pi^+\pi^-$ where both pions are misidentified as muons, is studied. The muon mass hypothesis is replaced by the pion mass, and the invariant-mass spectrum is analysed. No candidates with reconstructed $m(\pi^+\pi^-)$ in the B^0 mass region are seen, therefore, the contribution from the $B^{*0}\to B^0\gamma$ decay is found to be negligible.

The fit is performed in the invariant-mass range $[4.60,\,6.20]\,\mathrm{GeV}/c^2$. The invariant-mass distribution is shown in figure 5 for all q^2 bins. The low-mass region is populated by partially reconstructed background, while the higher mass region is dominated by combinatorial background. The sources of systematic uncertainties introduced in sections 4–5.1 are included in the fit as nuisance parameters, where the neutral PID and the differences between data and simulation are the dominant sources.

6 Results

The branching fraction of the signal decay is determined using an unbinned extended maximum-likelihood fit to the invariant-mass distribution of the contributions. The resulting branching fractions are

$$\begin{aligned}
\mathcal{B}(B_s^0\to\mu^+\mu^-\gamma)_{\mathrm{I}} &= (1.34\pm1.60\pm0.28)\times10^{-8},\\
\mathcal{B}(B_s^0\to\mu^+\mu^-\gamma)_{\mathrm{II}} &= (0.76\pm3.55\pm0.30)\times10^{-8},\\
\mathcal{B}(B_s^0\to\mu^+\mu^-\gamma)_{\mathrm{III}} &= (-2.55\pm2.25\pm0.41)\times10^{-8},\\
\mathcal{B}(B_s^0\to\mu^+\mu^-\gamma)_{\mathrm{I,\ with\ }\phi\mathrm{\ veto}} &= (0.72\pm1.56\pm0.29)\times10^{-8}.
\end{aligned}$$

JHEP07(2024)101

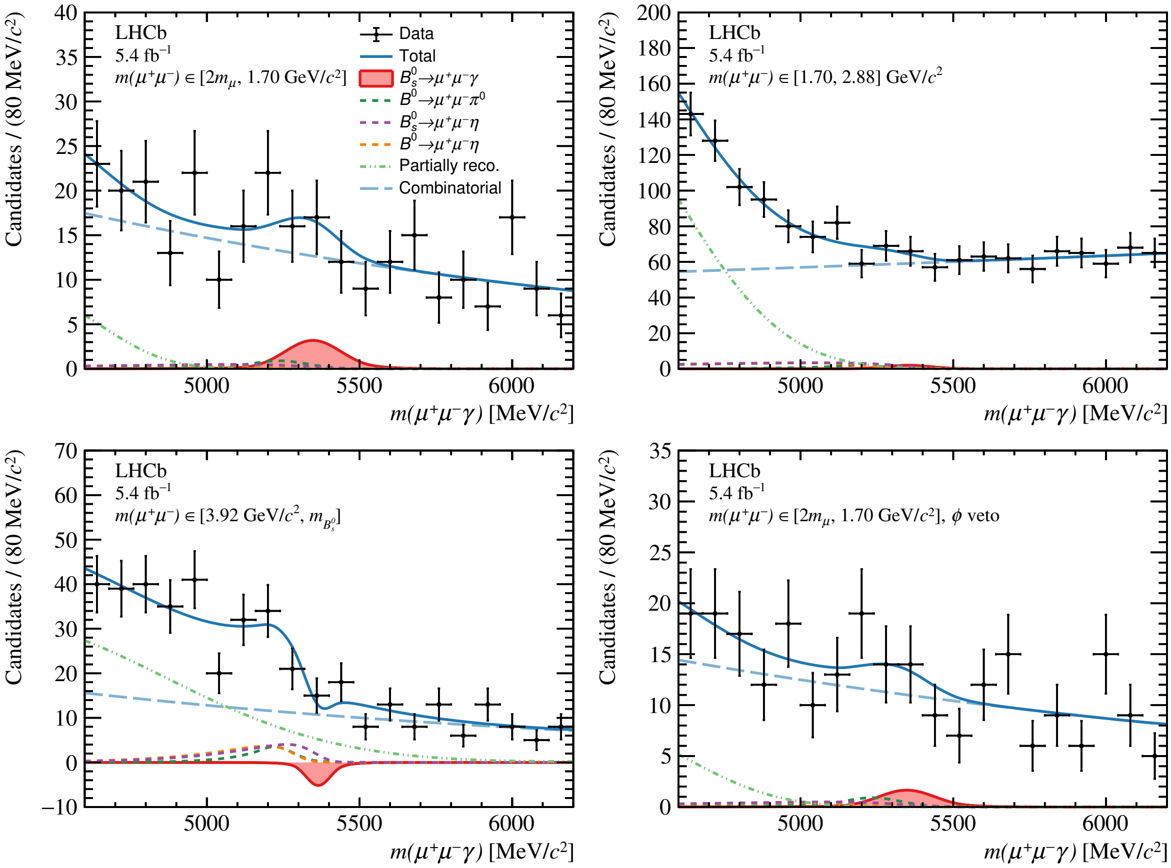

Figure 5. Mass distribution of signal candidates in regions of q^2, (top-left) bin I, (top-right) bin II, (bottom-left) bin III, and (bottom-right) ϕ-veto bin. The result of the fit is overlaid and the different components detailed in the legend.

The statistical uncertainties are evaluated by repeating the fits with all nuisance parameters fixed to the values obtained in the standard fit, where all nuisance parameters are free to float within their constraints. The systematic uncertainties are computed by subtracting the statistical uncertainties in quadrature from those obtained with the nuisance parameters floating.

The signal branching fractions are consistent with zero in all q^2 regions and consistent with the background-only hypothesis at the $< 1\sigma$ level. Limits are set on $\mathcal{B}(B_s^0 \to \mu^+\mu^-\gamma)$ using the $\mathrm{CL_s}$ method [54] with a one-sided test statistic [55] as implemented in refs. [56–58]. The one-sided test statistic for a given branching fraction value is defined as twice the negative logarithm of the profile likelihood ratio if it is larger than the measured branching fraction and zero otherwise. Its distribution is determined from pseudoexperiments, where nuisance parameters are set to their best fit values when generating the samples, while central values of the Gaussian-constraints are independently fluctuated within their uncertainty for each pseudoexperiment as described in ref. [59].

The fit is also performed simultaneously in the three q^2 regions to obtain a combined branching fraction limit. The $\mathrm{CL_s}$ curves are shown in figure 6 from which the limit on the

JHEP07(2024)101

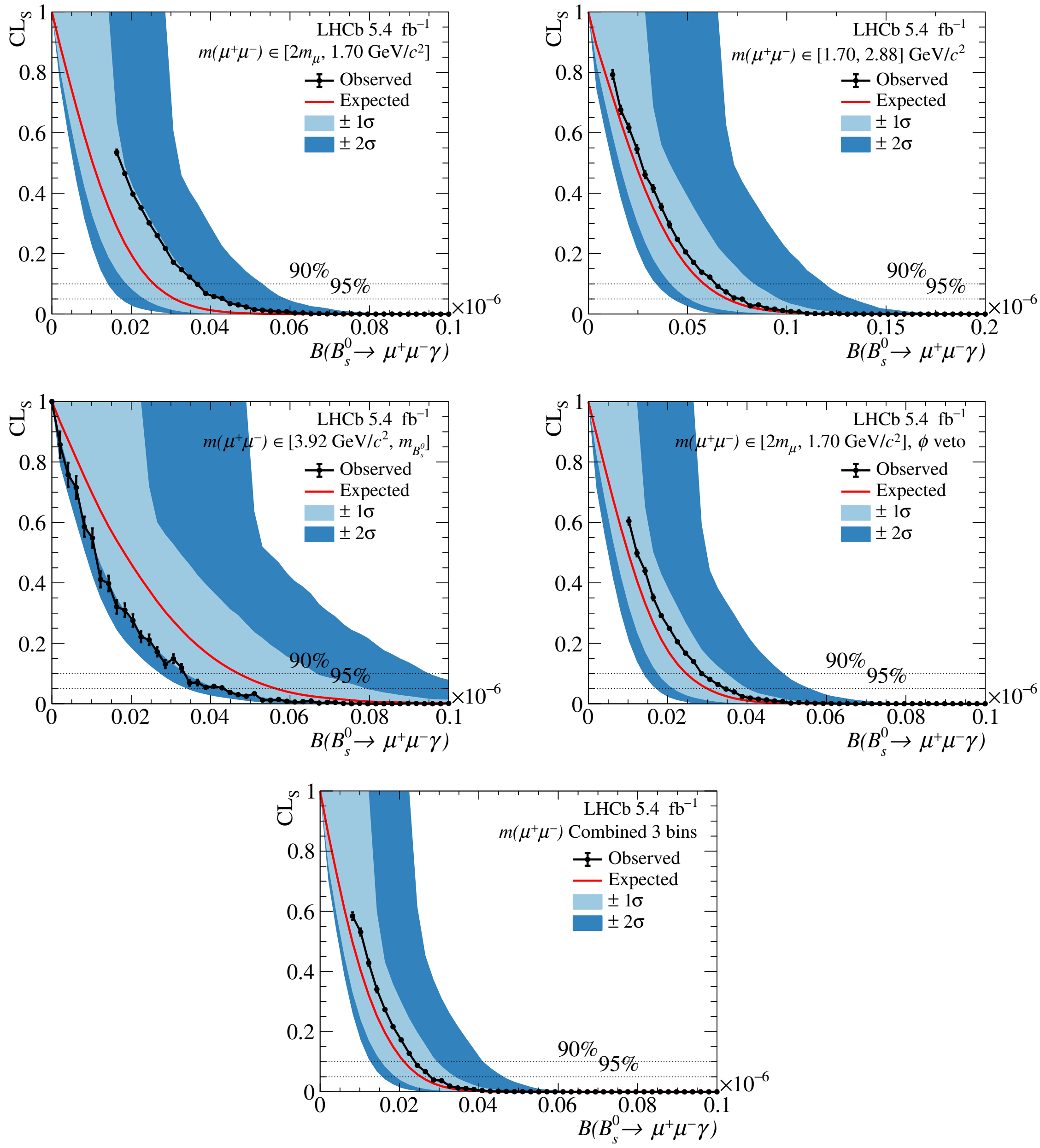

Figure 6. Results from the $\mathrm{CL_s}$ scan used to obtain the limit on $\mathcal{B}(B_s^0 \to \mu^+\mu^-\gamma)$ in regions of q^2: (top-left) bin I, (top-right) bin II, (middle-left) bin III, (middle-right) bin I with ϕ veto, and (bottom) the whole q^2 range. The background-only expectation is shown by the red line and the 1σ and 2σ bands are shown as light blue and blue bands, respectively. The observed limit is shown as the solid black line. The two dashed lines intersecting with the observation indicate the limits at 90% and 95% CL for the upper and lower line, respectively.

JHEP07(2024)101

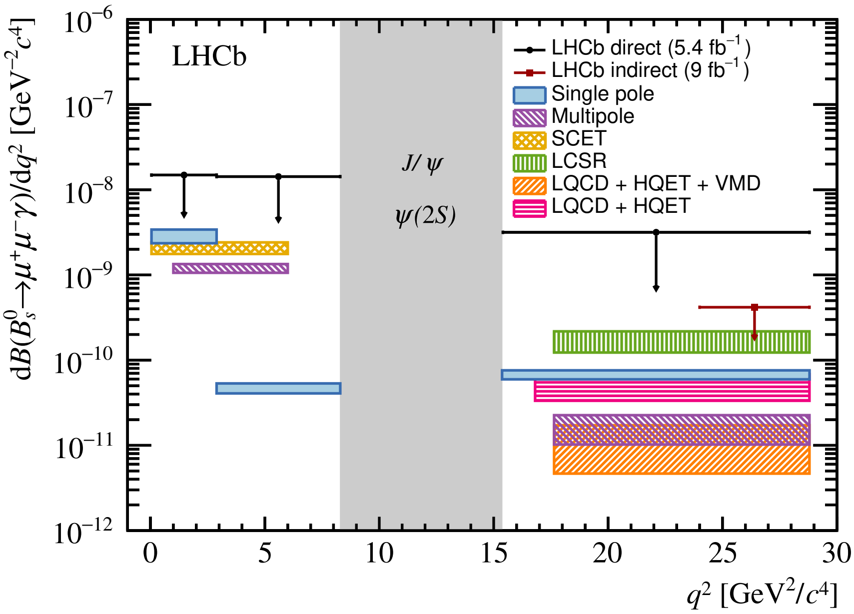

Figure 7. Differential branching fraction of the $B_s^0 \to \mu^+\mu^-\gamma$ decay in intervals of q^2. The black arrows represent the limits set in this paper at 95% CL. The limit set in the high-q^2 region with the indirect method from the $B_s^0 \to \mu^+\mu^-$ measurement at 95% CL is represented in red [18]. SM predictions using different form factor calculations are represented in (blue) ref. [9], (violet) ref. [10], (yellow) ref. [11], (green) ref. [12], (orange) refs. [14, 15], and (pink) ref. [13].

branching fraction for each q^2 region is found to be

$$\begin{aligned}
\mathcal{B}(B_s^0 \to \mu^+\mu^-\gamma)_{\mathrm{I}} &< 3.6\,(4.2) \times 10^{-8}, \\
\mathcal{B}(B_s^0 \to \mu^+\mu^-\gamma)_{\mathrm{II}} &< 6.5\,(7.7) \times 10^{-8}, \\
\mathcal{B}(B_s^0 \to \mu^+\mu^-\gamma)_{\mathrm{III}} &< 3.4\,(4.2) \times 10^{-8}, \\
\mathcal{B}(B_s^0 \to \mu^+\mu^-\gamma)_{\mathrm{I,\ with\ }\phi\mathrm{\ veto}} &< 2.9\,(3.4) \times 10^{-8}, \\
\mathcal{B}(B_s^0 \to \mu^+\mu^-\gamma)_{\mathrm{comb.}} &< 2.5\,(2.8) \times 10^{-8},
\end{aligned}$$

at 90% (95%) CL. The observed upper limits are shown in figure 6, together with the background-only expectations.

The limits are shown in figure 7, together with the limit set by the indirect method [18] for the $m(\mu^+\mu^-)$ range $[4.9,\, m_{B_s^0}]\,\mathrm{GeV}/c^2$. They are consistent with all SM predictions. The different theoretical approaches to the local form factor calculations predict different branching fractions, which are also shown in figure 7 as coloured bands. The theoretical predictions shown are calculated by a single-pole [9] and multipole [10] parametrisation, using SCET [11], from LCSR [12], and from lattice QCD using HQET extrapolation [13] and assuming VMD [14, 15].

7 Conclusions

In summary, data collected with the LHCb detector in the years 2016–2018, corresponding to an integrated luminosity of 5.4 fb^{-1} of proton-proton (pp) collisions at a center-of-mass energy

JHEP07(2024)101

$\sqrt{s} = 13\,\text{TeV}$ are analysed to search for the $B_s^0 \to \mu^+\mu^-\gamma$ decay. The search is performed in four regions of the dimuon invariant mass.

The measured signal is not statistically significant, and consistent with the background-only hypothesis at less than 1σ level in all dimuon mass regions. Upper limits on the branching fractions are set at

$$\begin{aligned}
\mathcal{B}(B_s^0 \to \mu^+\mu^-\gamma) &< 4.2 \times 10^{-8}, \quad m(\mu^+\mu^-) \in [2m_\mu,\ 1.70]\,\text{GeV}/c^2,\\
\mathcal{B}(B_s^0 \to \mu^+\mu^-\gamma) &< 7.7 \times 10^{-8}, \quad m(\mu^+\mu^-) \in [1.70,\ 2.88]\,\text{GeV}/c^2,\\
\mathcal{B}(B_s^0 \to \mu^+\mu^-\gamma) &< 4.2 \times 10^{-8}, \quad m(\mu^+\mu^-) \in [3.92,\ m_{B_s^0}]\,\text{GeV}/c^2,
\end{aligned}$$

and

$$\mathcal{B}(B_s^0 \to \mu^+\mu^-\gamma) < 2.8 \times 10^{-8}$$

for the combined dimuon mass regions, at 95% CL. Additionally, an upper limits are set at $\mathcal{B}(B_s^0 \to \mu^+\mu^-\gamma) < 3.4 \times 10^{-8}$ in the $[2m_\mu,\ 1.70]\,\text{GeV}/c^2$ dimuon mass region excluding the contribution from the intermediate ϕ meson. These are the first limits set on the $B_s^0 \to \mu^+\mu^-\gamma$ decay with full final state reconstruction and the first limit at dimuon masses below $4.9\,\text{GeV}/c^2$.

Acknowledgments

We express our gratitude to our colleagues in the CERN accelerator departments for the excellent performance of the LHC. We thank the technical and administrative staff at the LHCb institutes. We acknowledge support from CERN and from the national agencies: CAPES, CNPq, FAPERJ and FINEP (Brazil); MOST and NSFC (China); CNRS/IN2P3 (France); BMBF, DFG and MPG (Germany); INFN (Italy); NWO (Netherlands); MNiSW and NCN (Poland); MCID/IFA (Romania); MICINN (Spain); SNSF and SER (Switzerland); NASU (Ukraine); STFC (United Kingdom); DOE NP and NSF (U.S.A.). We acknowledge the computing resources that are provided by CERN, IN2P3 (France), KIT and DESY (Germany), INFN (Italy), SURF (Netherlands), PIC (Spain), GridPP (United Kingdom), CSCS (Switzerland), IFIN-HH (Romania), CBPF (Brazil), and Polish WLCG (Poland). We are indebted to the communities behind the multiple open-source software packages on which we depend. Individual groups or members have received support from ARC and ARDC (Australia); Key Research Program of Frontier Sciences of CAS, CAS PIFI, CAS CCEPP, Fundamental Research Funds for the Central Universities, and Sci. & Tech. Program of Guangzhou (China); Minciencias (Colombia); EPLANET, Marie Skłodowska-Curie Actions, ERC and NextGenerationEU (European Union); A*MIDEX, ANR, IPhU and Labex P2IO, and Région Auvergne-Rhône-Alpes (France); AvH Foundation (Germany); ICSC (Italy); GVA, XuntaGal, GENCAT, Inditex, InTalent and Prog. Atracción Talento, CM (Spain); SRC (Sweden); the Leverhulme Trust, the Royal Society and UKRI (United Kingdom).

References

[1] K.G. Wilson and J.B. Kogut, *The renormalization group and the ϵ expansion*, *Phys. Rept.* **12** (1974) 75 [INSPIRE].

[2] A. Greljo, J. Salko, A. Smolkovič and P. Stangl, *Rare b decays meet high-mass Drell-Yan*, *JHEP* **05** (2023) 087 [arXiv:2212.10497] [INSPIRE].

[3] M. Reboud, *The discrepancies in $b \to s$ semi-leptonic decays: A complete study from model-building aspects, to the definition of novel observables, to their measurement with the LHCb detector*, CERN-THESIS-2020-303 (2020).

[4] T.M. Aliev, A. Özpineci and M. Savcı, *Rare $B \to l^+l^-\gamma$ decay and new physics effects*, *Phys. Lett. B* **520** (2001) 69 [hep-ph/0105279] [INSPIRE].

[5] A.J. Buras and M. Münz, *Effective hamiltonian for $B \to X_s e^+e^-$ beyond leading logarithms in the naive dimensional regularization and 't Hooft-Veltman schemes*, *Phys. Rev. D* **52** (1995) 186 [hep-ph/9501281] [INSPIRE].

[6] G. Buchalla, A.J. Buras and M.E. Lautenbacher, *Weak decays beyond leading logarithms*, *Rev. Mod. Phys.* **68** (1996) 1125 [hep-ph/9512380] [INSPIRE].

[7] T.M. Aliev, A. Özpineci and M. Savcı, *$B_q \to l^+l^-\gamma$ decays in light cone QCD*, *Phys. Rev. D* **55** (1997) 7059 [hep-ph/9611393] [INSPIRE].

[8] Y. Dincer and L.M. Sehgal, *Charge asymmetry and photon energy spectrum in the decay $B_s \to l^+l^-\gamma$*, *Phys. Lett. B* **521** (2001) 7 [hep-ph/0108144] [INSPIRE].

[9] D. Guadagnoli, M. Reboud and R. Zwicky, *$B_s^0 \to \ell^+\ell^-\gamma$ as a Test of Lepton Flavor Universality*, *JHEP* **11** (2017) 184 [arXiv:1708.02649] [INSPIRE].

[10] A. Kozachuk, D. Melikhov and N. Nikitin, *Rare FCNC radiative leptonic $B_{s,d} \to \gamma l^+l^-$ decays in the standard model*, *Phys. Rev. D* **97** (2018) 053007 [arXiv:1712.07926] [INSPIRE].

[11] M. Beneke, C. Bobeth and Y.-M. Wang, *$B_{d,s} \to \gamma\ell\ell$ decay with an energetic photon*, *JHEP* **12** (2020) 148 [arXiv:2008.12494] [INSPIRE].

[12] T. Janowski, B. Pullin and R. Zwicky, *Charged and neutral $B_{u,d,s} \to \gamma$ form factors from light cone sum rules at NLO*, *JHEP* **12** (2021) 008 [arXiv:2106.13616] [INSPIRE].

[13] R. Frezzotti et al., *The $B_s \to \mu^+\mu^-\gamma$ decay rate at large q^2 from lattice QCD*, *Phys. Rev. D* **109** (2024) 114506 [arXiv:2402.03262] [INSPIRE].

[14] D. Guadagnoli, C. Normand, S. Simula and L. Vittorio, *Insights on the current semi-leptonic B-decay discrepancies — and how $B_s \to \mu^+\mu^-\gamma$ can help*, *JHEP* **10** (2023) 102 [arXiv:2308.00034] [INSPIRE].

[15] D. Guadagnoli, C. Normand, S. Simula and L. Vittorio, *From $D_s \to \gamma$ in lattice QCD to $B_s \to \mu\mu\gamma$ at high q^2*, *JHEP* **07** (2023) 112 [arXiv:2303.02174] [INSPIRE].

[16] D. Melikhov and N. Nikitin, *Rare radiative leptonic decays $B_{d,s} \to \ell^+\ell^-\gamma$*, *Phys. Rev. D* **70** (2004) 114028 [hep-ph/0410146] [INSPIRE].

[17] BaBar collaboration, *Search for the decays $B^0 \to e^+e^-\gamma$ and $B^0 \to \mu^+\mu^-\gamma$*, *Phys. Rev. D* **77** (2008) 011104 [arXiv:0706.2870] [INSPIRE].

[18] LHCb collaboration, *Measurement of the $B_s^0 \to \mu^+\mu^-$ decay properties and search for the $B^0 \to \mu^+\mu^-$ and $B_s^0 \to \mu^+\mu^-\gamma$ decays*, *Phys. Rev. D* **105** (2022) 012010 [arXiv:2108.09283] [INSPIRE].

JHEP07(2024)101

[19] A. Carvunis et al., *On the effective lifetime of $B_s \to \mu\mu\gamma$*, *JHEP* **12** (2021) 078 [arXiv:2102.13390] [INSPIRE].

[20] TMVA collaboration, *TMVA 4 — Toolkit for Multivariate Data Analysis with ROOT. Users Guide*, physics/0703039 [INSPIRE].

[21] H. Voss, A. Höcker, J. Stelzer and F. Tegenfeldt, *TMVA, the Toolkit for Multivariate Data Analysis with ROOT*, *PoS* **ACAT** (2007) 040 [physics/0703039] [INSPIRE].

[22] LHCb collaboration, *The LHCb detector at the LHC*, 2008 *JINST* **3** S08005 [INSPIRE].

[23] LHCb collaboration, *LHCb detector performance*, *Int. J. Mod. Phys. A* **30** (2015) 1530022 [arXiv:1412.6352] [INSPIRE].

[24] R. Aaij et al., *Performance of the LHCb Vertex Locator*, 2014 *JINST* **9** P09007 [arXiv:1405.7808] [INSPIRE].

[25] LHCb Outer Tracker Group collaboration, *Improved performance of the LHCb Outer Tracker in LHC Run 2*, 2017 *JINST* **12** P11016 [arXiv:1708.00819] [INSPIRE].

[26] LHCb RICH Group collaboration, *Performance of the LHCb RICH detector at the LHC*, *Eur. Phys. J. C* **73** (2013) 2431 [arXiv:1211.6759] [INSPIRE].

[27] A.A. Alves Jr. et al., *Performance of the LHCb muon system*, 2013 *JINST* **8** P02022 [arXiv:1211.1346] [INSPIRE].

[28] R. Aaij et al., *The LHCb trigger and its performance in 2011*, 2013 *JINST* **8** P04022 [arXiv:1211.3055] [INSPIRE].

[29] T. Sjöstrand, S. Mrenna and P.Z. Skands, *A brief introduction to PYTHIA 8.1*, *Comput. Phys. Commun.* **178** (2008) 852 [arXiv:0710.3820] [INSPIRE].

[30] T. Sjöstrand, S. Mrenna and P.Z. Skands, *PYTHIA 6.4 physics and manual*, *JHEP* **05** (2006) 026 [hep-ph/0603175] [INSPIRE].

[31] LHCb collaboration, *Handling of the generation of primary events in Gauss, the LHCb simulation framework*, *J. Phys. Conf. Ser.* **331** (2011) 032047 [INSPIRE].

[32] D.J. Lange, *The EvtGen particle decay simulation package*, *Nucl. Instrum. Meth. A* **462** (2001) 152 [INSPIRE].

[33] N. Davidson, T. Przedzinski and Z. Was, *PHOTOS interface in C++: Technical and physics documentation*, *Comput. Phys. Commun.* **199** (2016) 86 [arXiv:1011.0937] [INSPIRE].

[34] J. Allison et al., *Geant4 developments and applications*, *IEEE Trans. Nucl. Sci.* **53** (2006) 270 [INSPIRE].

[35] GEANT4 collaboration, *Geant4: A simulation toolkit*, *Nucl. Instrum. Meth. A* **506** (2003) 250 [INSPIRE].

[36] LHCb collaboration, *The LHCb simulation application, Gauss: Design, evolution and experience*, *J. Phys. Conf. Ser.* **331** (2011) 032023 [INSPIRE].

[37] T. Likhomanenko et al., *LHCb topological trigger reoptimization*, *J. Phys. Conf. Ser.* **664** (2015) 082025 [arXiv:1510.00572] [INSPIRE].

[38] C. Abellán Beteta et al., *Calibration and performance of the LHCb calorimeters in Run 1 and 2 at the LHC*, arXiv:2008.11556 [INSPIRE].

[39] Particle Data Group collaboration, *Review of particle physics*, *PTEP* **2022** (2022) 083C01 [INSPIRE].

[40] F. Archilli et al., *Performance of the Muon Identification at LHCb*, 2013 *JINST* **8** P10020 [arXiv:1306.0249] [INSPIRE].

[41] O. Deschamps et al., *Photon and neutral pion reconstruction*, LHCb-2003-091 (2003) [INSPIRE].

[42] W.S. McCulloch and W. Pitts, *A logical calculus of the ideas immanent in nervous activity*, *Bull. Math. Biol.* **5** (1943) 115 [INSPIRE].

[43] F. Rosenblatt, *The perceptron: A probabilistic model for information storage and organization in the brain*, *Psychol. Rev.* **65** (1958) 386.

[44] J.-H. Zhong et al., *A program for the Bayesian neural network in the ROOT framework*, *Comput. Phys. Commun.* **182** (2011) 2655 [arXiv:1103.2854] [INSPIRE].

[45] G. Punzi, *Sensitivity of searches for new signals and its optimization*, *eConf C* **030908** (2003) MODT002 [physics/0308063] [INSPIRE].

[46] LHCb collaboration, *First observation of the radiative $\Lambda_b^0 \to \Lambda\gamma$ decay*, *Phys. Rev. Lett.* **123** (2019) 031801 [arXiv:1904.06697] [INSPIRE].

[47] LHCb collaboration, *Search for the radiative $\Xi_b^- \to \Xi^-\gamma$ decay*, *JHEP* **01** (2022) 069 [arXiv:2108.07678] [INSPIRE].

[48] T. Skwarnicki, *A study of the radiative CASCADE transitions between the Upsilon-Prime and Upsilon resonances*, Ph.D. Thesis, Institute of Nuclear Physics, Kraków (1986) [INSPIRE].

[49] ARGUS collaboration, *Search for hadronic $b \to u$ decays*, *Phys. Lett. B* **241** (1990) 278 [arXiv:2206.06673] [INSPIRE].

[50] M. Pivk and F.R. Le Diberder, *sPlot: A statistical tool to unfold data distributions*, *Nucl. Instrum. Meth. A* **555** (2005) 356 [physics/0402083] [INSPIRE].

[51] A. Rogozhnikov, *Reweighting with Boosted Decision Trees*, *J. Phys. Conf. Ser.* **762** (2016) 012036 [https://github.com/arogozhnikov/hep_ml] [arXiv:1608.05806] [INSPIRE].

[52] L. Anderlini et al., *The PIDCalib package*, LHCb-PUB-2016-021 (2016).

[53] S. Tolk, J. Albrecht, F. Dettori and A. Pellegrino, *Data driven trigger efficiency determination at LHCb*, LHCb-PUB-2014-039 (2014).

[54] A.L. Read, *Presentation of search results: The CL_s technique*, *J. Phys. G* **28** (2002) 2693 [INSPIRE].

[55] G. Cowan, K. Cranmer, E. Gross and O. Vitells, *Asymptotic formulae for likelihood-based tests of new physics*, *Eur. Phys. J. C* **71** (2011) 1554 [*Erratum ibid.* **73** (2013) 2501] [arXiv:1007.1727] [INSPIRE].

[56] M. Kenzie et al., *GammaCombo: A statistical analysis framework for combining measurements, fitting datasets and producing confidence intervals*, DOI:10.5281/zenodo.3371421.

[57] LHCb collaboration, *Simultaneous determination of CKM angle γ and charm mixing parameters*, *JHEP* **12** (2021) 141 [arXiv:2110.02350] [INSPIRE].

[58] LHCb collaboration, *Measurement of the CKM angle γ from a combination of LHCb results*, *JHEP* **12** (2016) 087 [arXiv:1611.03076] [INSPIRE].

[59] S. Bodhisattva, M. Walker and M. Woodroofe, *On the Unified Method with Nuisance Parameters*, *Statist. Sinica* **19** (2009) 301 [INSPIRE].

The LHCb collaboration

R. Aaij[35], A.S.W. Abdelmotteleb[54], C. Abellan Beteta[48], F. Abudinén[54], T. Ackernley[58], A.
A. Adefisoye[66], B. Adeva[44], M. Adinolfi[52], P. Adlarson[79], C. Agapopoulou[46],
C.A. Aidala[80], Z. Ajaltouni[11], S. Akar[63], K. Akiba[35], P. Albicocco[25], J. Albrecht[17],
F. Alessio[46], M. Alexander[57], Z. Aliouche[60], P. Alvarez Cartelle[53], R. Amalric[15],
S. Amato[3], J.L. Amey[52], Y. Amhis[13,46], L. An[6], L. Anderlini[24], M. Andersson[48],
A. Andreianov[41], P. Andreola[48], M. Andreotti[23], D. Andreou[66], A. Anelli[28,p], D. Ao[7],
F. Archilli[34,v], M. Argenton[23], S. Arguedas Cuendis[9], A. Artamonov[41], M. Artuso[66],
E. Aslanides[12], M. Atzeni[62], B. Audurier[14], D. Bacher[61], I. Bachiller Perea[10],
S. Bachmann[19], M. Bachmayer[47], J.J. Back[54], P. Baladron Rodriguez[44], V. Balagura[14],
W. Baldini[23], J. Baptista de Souza Leite[58], M. Barbetti[24,m], I. R. Barbosa[67],
R.J. Barlow[60], S. Barsuk[13], W. Barter[56], M. Bartolini[53], J. Bartz[66], F. Baryshnikov[41],
J.M. Basels[16], G. Bassi[32], B. Batsukh[5], A. Battig[17], A. Bay[47], A. Beck[54],
M. Becker[17], F. Bedeschi[32], I.B. Bediaga[2], A. Beiter[66], S. Belin[44], V. Bellee[48],
K. Belous[41], I. Belov[26], I. Belyaev[33], G. Benane[12], G. Bencivenni[25], E. Ben-Haim[15],
A. Berezhnoy[41], R. Bernet[48], S. Bernet Andres[42], C. Bertella[60], A. Bertolin[30],
C. Betancourt[48], F. Betti[56], J. Bex[53], Ia. Bezshyiko[48], J. Bhom[38], M.S. Bieker[17],
N.V. Biesuz[23], P. Billoir[15], A. Biolchini[35], M. Birch[59], F.C.R. Bishop[10], A. Bitadze[60],
A. Bizzeti, T. Blake[54], F. Blanc[47], J.E. Blank[17], S. Blusk[66], V. Bocharnikov[41],
J.A. Boelhauve[17], O. Boente Garcia[14], T. Boettcher[63], A. Bohare[56], A. Boldyrev[41],
C.S. Bolognani[76], R. Bolzonella[23,l], N. Bondar[41], F. Borgato[30,q,46], S. Borghi[60],
M. Borsato[28,p], J.T. Borsuk[38], S.A. Bouchiba[47], T.J.V. Bowcock[58], A. Boyer[46],
C. Bozzi[23], M.J. Bradley[59], A. Brea Rodriguez[44], N. Breer[17], J. Brodzicka[38],
A. Brossa Gonzalo[44], J. Brown[58], D. Brundu[29], E. Buchanan[56], A. Buonaura[48],
L. Buonincontri[30,q], A.T. Burke[60], C. Burr[46], A. Bursche[69], A. Butkevich[41], J.S. Butter[53],
J. Buytaert[46], W. Byczynski[46], S. Cadeddu[29], H. Cai[71], R. Calabrese[23,l], L. Calefice[43],
S. Cali[25], M. Calvi[28,p], M. Calvo Gomez[42], J. I. Cambon Bouzas[44], P. Campana[25],
D.H. Campora Perez[76], A.F. Campoverde Quezada[7], S. Capelli[28,p], L. Capriotti[23],
R. Caravaca-Mora[9], A. Carbone[22,j], L. Carcedo Salgado[44], R. Cardinale[26,n], A. Cardini[29],
P. Carniti[28,p], L. Carus[19], A. Casais Vidal[62], R. Caspary[19], G. Casse[58],
J. Castro Godinez[9], M. Cattaneo[46], G. Cavallero[23], V. Cavallini[23,l], S. Celani[19],
J. Cerasoli[12], D. Cervenkov[61], S. Cesare[27,o], A.J. Chadwick[58], I. Chahrour[80],
M. Charles[15], Ph. Charpentier[46], C.A. Chavez Barajas[58], M. Chefdeville[10], C. Chen[12],
S. Chen[5], Z. Chen[7], A. Chernov[38], S. Chernyshenko[50], V. Chobanova[78], S. Cholak[47],
M. Chrzaszcz[38], A. Chubykin[41], V. Chulikov[41], P. Ciambrone[25], X. Cid Vidal[44],
G. Ciezarek[46], P. Cifra[46], P.E.L. Clarke[56], M. Clemencic[46], H.V. Cliff[53], J. Closier[46],
C. Cocha Toapaxi[19], V. Coco[46], J. Cogan[12], E. Cogneras[11], L. Cojocariu[40], P. Collins[46],
T. Colombo[46], A. Comerma-Montells[43], L. Congedo[21], A. Contu[29], N. Cooke[57],
I. Corredoira [44], A. Correia[15], G. Corti[46], J.J. Cottee Meldrum[52], B. Couturier[46],
D.C. Craik[48], M. Cruz Torres[2,g], E. Curras Rivera[47], R. Currie[56], C.L. Da Silva[65],
S. Dadabaev[41], L. Dai[68], X. Dai[6], E. Dall'Occo[17], J. Dalseno[44], C. D'Ambrosio[46],
J. Daniel[11], A. Danilina[41], P. d'Argent[21], A. Davidson[54], J.E. Davies[60], A. Davis[60],

JHEP07(2024)101

O. De Aguiar Francisco[60], C. De Angelis[29,k], F. De Benedetti[46], J. de Boer[35], K. De Bruyn[75], S. De Capua[60], M. De Cian[19,46], U. De Freitas Carneiro Da Graca[2,b], E. De Lucia[25], J.M. De Miranda[2], L. De Paula[3], M. De Serio[21,h], D. De Simone[48], P. De Simone[25], F. De Vellis[17], J.A. de Vries[76], F. Debernardis[21], D. Decamp[10], V. Dedu[12], L. Del Buono[15], B. Delaney[62], H.-P. Dembinski[17], J. Deng[8], V. Denysenko[48], O. Deschamps[11], F. Dettori[29,k], B. Dey[74], P. Di Nezza[25], I. Diachkov[41], S. Didenko[41], S. Ding[66], L. Dittmann[19], V. Dobishuk[50], A. D. Docheva[57], A. Dolmatov[41], C. Dong[4], A.M. Donohoe[20], F. Dordei[29], A.C. dos Reis[2], A. D. Dowling[66], A.G. Downes[10], W. Duan[69], P. Duda[77], M.W. Dudek[38], L. Dufour[46], V. Duk[31], P. Durante[46], M. M. Duras[77], J.M. Durham[65], O. D. Durmus[74], A. Dziurda[38], A. Dzyuba[41], S. Easo[55], E. Eckstein[73], U. Egede[1], A. Egorychev[41], V. Egorychev[41], S. Eisenhardt[56], E. Ejopu[60], S. Ek-In[47], L. Eklund[79], M. Elashri[63], J. Ellbracht[17], S. Ely[59], A. Ene[40], E. Epple[63], S. Escher[16], J. Eschle[48], S. Esen[19], T. Evans[60], F. Fabiano[29,k,46], L.N. Falcao[2], Y. Fan[7], B. Fang[71,13], L. Fantini[31,r], M. Faria[47], K. Farmer[56], D. Fazzini[28,p], L. Felkowski[77], M. Feng[5,7], M. Feo[46], M. Fernandez Gomez[44], A.D. Fernez[64], F. Ferrari[22], F. Ferreira Rodrigues[3], S. Ferreres Sole[35], M. Ferrillo[48], M. Ferro-Luzzi[46], S. Filippov[41], R.A. Fini[21], M. Fiorini[23,l], K.M. Fischer[61], D.S. Fitzgerald[80], C. Fitzpatrick[60], F. Fleuret[14], M. Fontana[22], L. F. Foreman[60], R. Forty[46], D. Foulds-Holt[53], M. Franco Sevilla[64], M. Frank[46], E. Franzoso[23,l], G. Frau[19], C. Frei[46], D.A. Friday[60], J. Fu[7], Q. Fuehring[17], Y. Fujii[1], T. Fulghesu[15], E. Gabriel[35], G. Galati[21,h], M.D. Galati[35], A. Gallas Torreira[44], D. Galli[22,j], S. Gambetta[56], M. Gandelman[3], P. Gandini[27], H. Gao[7], R. Gao[61], Y. Gao[8], Y. Gao[6], Y. Gao[8], M. Garau[29,k], L.M. Garcia Martin[47], P. Garcia Moreno[43], J. García Pardiñas[46], K. G. Garg[8], L. Garrido[43], C. Gaspar[46], R.E. Geertsema[35], L.L. Gerken[17], E. Gersabeck[60], M. Gersabeck[60], T. Gershon[54], Z. Ghorbanimoghaddam[52], L. Giambastiani[30,q], F. I. Giasemis[15,e], V. Gibson[53], H.K. Giemza[39], A.L. Gilman[61], M. Giovannetti[25], A. Gioventù[43], P. Gironella Gironell[43], C. Giugliano[23,l], M.A. Giza[38], E.L. Gkougkousis[59], F.C. Glaser[13,19], V.V. Gligorov[15], C. Göbel[67], E. Golobardes[42], D. Golubkov[41], A. Golutvin[59,41,46], A. Gomes[2,a,†], S. Gomez Fernandez[43], F. Goncalves Abrantes[61], M. Goncerz[38], G. Gong[4], J. A. Gooding[17], I.V. Gorelov[41], C. Gotti[28], J.P. Grabowski[73], L.A. Granado Cardoso[46], E. Graugés[43], E. Graverini[47,t], L. Grazette[54], G. Graziani, A. T. Grecu[40], L.M. Greeven[35], N.A. Grieser[63], L. Grillo[57], S. Gromov[41], C. Gu[14], M. Guarise[23], M. Guittiere[13], V. Guliaeva[41], P. A. Günther[19], A.-K. Guseinov[47], E. Gushchin[41], Y. Guz[6,41,46], T. Gys[46], K. Habermann[73], T. Hadavizadeh[1], C. Hadjivasiliou[64], G. Haefeli[47], C. Haen[46], J. Haimberger[46], M. Hajheidari[46], M.M. Halvorsen[46], P.M. Hamilton[64], J. Hammerich[58], Q. Han[8], X. Han[19], S. Hansmann-Menzemer[19], L. Hao[7], N. Harnew[61], T. Harrison[58], M. Hartmann[13], J. He[7,c], K. Heijhoff[35], F. Hemmer[46], C. Henderson[63], R.D.L. Henderson[1,54], A.M. Hennequin[46], K. Hennessy[58], L. Henry[47], J. Herd[59], P. Herrero Gascon[19], J. Heuel[16], A. Hicheur[3], G. Hijano Mendizabal[48], D. Hill[47], S.E. Hollitt[17], J. Horswill[60], R. Hou[8], Y. Hou[10], N. Howarth[58], J. Hu[19], J. Hu[69], W. Hu[6], X. Hu[4], W. Huang[7], W. Hulsbergen[35], R.J. Hunter[54], M. Hushchyn[41], D. Hutchcroft[58], D. Ilin[41], P. Ilten[63], A. Inglessi[41], A. Iniukhin[41], A. Ishteev[41], K. Ivshin[41], R. Jacobsson[46], H. Jage[16], S.J. Jaimes Elles[45,72], S. Jakobsen[46], E. Jans[35], B.K. Jashal[45], A. Jawahery[64,46], V. Jevtic[17], E. Jiang[64], X. Jiang[5,7], Y. Jiang[7], Y. J. Jiang[6], M. John[61], D. Johnson[51], C.R. Jones[53], T.P. Jones[54], S. Joshi[39], B. Jost[46], N. Jurik[46], I. Juszczak[38], D. Kaminaris[47], S. Kandybei[49], Y. Kang[4], M. Karacson[46], D. Karpenkov[41], A. Kauniskangas[47], J.W. Kautz[63], F. Keizer[46], M. Kenzie[53], T. Ketel[35], B. Khanji[66], A. Kharisova[41], S. Kholodenko[32], G. Khreich[13], T. Kirn[16], V.S. Kirsebom[28,p], O. Kitouni[62], S. Klaver[36], N. Kleijne[32,s], K. Klimaszewski[39], M.R. Kmiec[39], S. Koliiev[50], L. Kolk[17], A. Konoplyannikov[41], P. Kopciewicz[37,46], P. Koppenburg[35], M. Korolev[41], I. Kostiuk[35], O. Kot[50], S. Kotriakhova, A. Kozachuk[41], P. Kravchenko[41], L. Kravchuk[41], M. Kreps[54], S. Kretzschmar[16], P. Krokovny[41], W. Krupa[66], W. Krzemien[39], J. Kubat[19], S. Kubis[77], W. Kucewicz[38], M. Kucharczyk[38], V. Kudryavtsev[41], E. Kulikova[41], A. Kupsc[79], B. K. Kutsenko[12], D. Lacarrere[46], A. Lai[29], A. Lampis[29], D. Lancierini[53], C. Landesa Gomez[44], J.J. Lane[1], R. Lane[52], C. Langenbruch[19], J. Langer[17], O. Lantwin[41], T. Latham[54], F. Lazzari[32,t], C. Lazzeroni[51], R. Le Gac[12], R. Lefèvre[11], A. Leflat[41], S. Legotin[41], M. Lehuraux[54], E. Lemos Cid[46], O. Leroy[12], T. Lesiak[38], B. Leverington[19], A. Li[4], H. Li[69], K. Li[8], L. Li[60], P. Li[46], P.-R. Li[70], S. Li[8], T. Li[5,d], T. Li[69], Y. Li[8], Y. Li[5], Z. Li[66], Z. Lian[4], X. Liang[66], S. Libralon[45], C. Lin[7], T. Lin[55], R. Lindner[46], V. Lisovskyi[47], R. Litvinov[29,k], F. L. Liu[1], G. Liu[69], K. Liu[70], Q. Liu[7], S. Liu[5,7], Y. Liu[56], Y. Liu[70], Y. L. Liu[59], A. Lobo Salvia[43], A. Loi[29], J. Lomba Castro[44], T. Long[53], J.H. Lopes[3], A. Lopez Huertas[43], S. López Soliño[44], G.H. Lovell[53], C. Lucarelli[24,m], D. Lucchesi[30,q], M. Lucio Martinez[76], V. Lukashenko[35,50], Y. Luo[6], A. Lupato[30], E. Luppi[23,l], K. Lynch[20], X.-R. Lyu[7], G. M. Ma[4], R. Ma[7], S. Maccolini[17], F. Machefert[13], F. Maciuc[40], B. M. Mack[66], I. Mackay[61], L. M. Mackey[66], L.R. Madhan Mohan[53], M. M. Madurai[51], A. Maevskiy[41], D. Magdalinski[35], D. Maisuzenko[41], M.W. Majewski[37], J.J. Malczewski[38], S. Malde[61], B. Malecki[38,46], L. Malentacca[46], A. Malinin[41], T. Maltsev[41], G. Manca[29,k], G. Mancinelli[12], C. Mancuso[27,13,o], R. Manera Escalero[43], D. Manuzzi[22], D. Marangotto[27,o], J.F. Marchand[10], R. Marchevski[47], U. Marconi[22], S. Mariani[46], C. Marin Benito[43], J. Marks[19], A.M. Marshall[52], P.J. Marshall[58], G. Martelli[31,r], G. Martellotti[33], L. Martinazzoli[46], M. Martinelli[28,p], D. Martinez Santos[44], F. Martinez Vidal[45], A. Massafferri[2], M. Materok[16], R. Matev[46], A. Mathad[46], V. Matiunin[41], C. Matteuzzi[66], K.R. Mattioli[14], A. Mauri[59], E. Maurice[14], J. Mauricio[43], P. Mayencourt[47], M. Mazurek[39], M. McCann[59], L. Mcconnell[20], T.H. McGrath[60], N.T. McHugh[57], A. McNab[60], R. McNulty[20], B. Meadows[63], G. Meier[17], D. Melnychuk[39], M. Merk[35,76], A. Merli[27,o], L. Meyer Garcia[3], D. Miao[5,7], H. Miao[7], M. Mikhasenko[73,f], D.A. Milanes[72], A. Minotti[28,p], E. Minucci[66], T. Miralles[11], B. Mitreska[17], D.S. Mitzel[17], A. Modak[55], A. Mödden [17], R.A. Mohammed[61], R.D. Moise[16], S. Mokhnenko[41], T. Mombächer[46], M. Monk[54,1], S. Monteil[11], A. Morcillo Gomez[44], G. Morello[25], M.J. Morello[32,s], M.P. Morgenthaler[19], A.B. Morris[46], A.G. Morris[12], R. Mountain[66], H. Mu[4], Z. M. Mu[6], E. Muhammad[54], F. Muheim[56], M. Mulder[75], K. Müller[48], F. Muñoz-Rojas[9], R. Murta[59], P. Naik[58], T. Nakada[47], R. Nandakumar[55], T. Nanut[46], I. Nasteva[3], M. Needham[56], N. Neri[27,o], S. Neubert[73], N. Neufeld[46], P. Neustroev[41], J. Nicolini[17,13], D. Nicotra[76], E.M. Niel[47], N. Nikitin[41],

JHEP07(2024)101

P. Nogga[73], N.S. Nolte[62], C. Normand[52], J. Novoa Fernandez[44], G. Nowak[63], C. Nunez[80], H. N. Nur[57], A. Oblakowska-Mucha[37], V. Obraztsov[41], T. Oeser[16], S. Okamura[23,l,46], A. Okhotnikov[41], R. Oldeman[29,k], F. Oliva[56], M. Olocco[17], C.J.G. Onderwater[76], R.H. O'Neil[56], J.M. Otalora Goicochea[3], P. Owen[48], A. Oyanguren[45], O. Ozcelik[56], K.O. Padeken[73], B. Pagare[54], P.R. Pais[19], T. Pajero[61], A. Palano[21], M. Palutan[25], G. Panshin[41], L. Paolucci[54], A. Papanestis[55], M. Pappagallo[21,h], L.L. Pappalardo[23,l], C. Pappenheimer[63], C. Parkes[60], B. Passalacqua[23], G. Passaleva[24], D. Passaro[32,s], A. Pastore[21], M. Patel[59], J. Patoc[61], C. Patrignani[22,j], C.J. Pawley[76], A. Pellegrino[35], M. Pepe Altarelli[25], S. Perazzini[22], D. Pereima[41], A. Pereiro Castro[44], P. Perret[11], A. Perro[46], K. Petridis[52], A. Petrolini[26,n], S. Petrucci[56], J. P. Pfaller[63], H. Pham[66], L. Pica[32,s], M. Piccini[31], B. Pietrzyk[10], G. Pietrzyk[13], D. Pinci[33], F. Pisani[46], M. Pizzichemi[28,p], V. Placinta[40], M. Plo Casasus[44], F. Polci[15,46], M. Poli Lener[25], A. Poluektov[12], N. Polukhina[41], I. Polyakov[46], E. Polycarpo[3], S. Ponce[46], D. Popov[7], S. Poslavskii[41], K. Prasanth[38], C. Prouve[44], V. Pugatch[50], G. Punzi[32,t], W. Qian[7], N. Qin[4], S. Qu[4], R. Quagliani[47], R.I. Rabadan Trejo[54], J.H. Rademacker[52], M. Rama[32], M. Ramírez García[80], M. Ramos Pernas[54], M.S. Rangel[3], F. Ratnikov[41], G. Raven[36], M. Rebollo De Miguel[45], M. Reboud[10], F. Redi[27,i], J. Reich[52], F. Reiss[60], Z. Ren[7], P.K. Resmi[61], R. Ribatti[32,s], G. R. Ricart[14,81], D. Riccardi[32,s], S. Ricciardi[55], K. Richardson[62], M. Richardson-Slipper[56], K. Rinnert[58], P. Robbe[13], G. Robertson[57], E. Rodrigues[58], E. Rodriguez Fernandez[44], J.A. Rodriguez Lopez[72], E. Rodriguez Rodriguez[44], A. Rogovskiy[55], D.L. Rolf[46], P. Roloff[46], V. Romanovskiy[41], M. Romero Lamas[44], A. Romero Vidal[44], G. Romolini[23], F. Ronchetti[47], M. Rotondo[25], S. R. Roy[19], M.S. Rudolph[66], T. Ruf[46], M. Ruiz Diaz[19], R.A. Ruiz Fernandez[44], J. Ruiz Vidal[79,z], A. Ryzhikov[41], J. Ryzka[37], J. J. Saavedra-Arias[9], J.J. Saborido Silva[44], R. Sadek[14], N. Sagidova[41], D. Sahoo[74], N. Sahoo[51], B. Saitta[29,k], M. Salomoni[28,p], C. Sanchez Gras[35], I. Sanderswood[45], R. Santacesaria[33], C. Santamarina Rios[44], M. Santimaria[25], L. Santoro[2], E. Santovetti[34], A. Saputi[23,46], D. Saranin[41], G. Sarpis[56], M. Sarpis[73], A. Sarti[33], C. Satriano[33,u], A. Satta[34], M. Saur[6], D. Savrina[41], H. Sazak[16], L.G. Scantlebury Smead[61], A. Scarabotto[17], S. Schael[16], S. Scherl[58], A. M. Schertz[74], M. Schiller[57], H. Schindler[46], M. Schmelling[18], B. Schmidt[46], S. Schmitt[16], H. Schmitz[73], O. Schneider[47], A. Schopper[46], N. Schulte[17], S. Schulte[47], M.H. Schune[13], R. Schwemmer[46], G. Schwering[16], B. Sciascia[25], A. Sciuccati[46], S. Sellam[44], A. Semennikov[41], T. Senger[48], M. Senghi Soares[36], A. Sergi[26], N. Serra[48], L. Sestini[30], A. Seuthe[17], Y. Shang[6], D.M. Shangase[80], M. Shapkin[41], R. S. Sharma[66], I. Shchemerov[41], L. Shchutska[47], T. Shears[58], L. Shekhtman[41], Z. Shen[6], S. Sheng[5,7], V. Shevchenko[41], B. Shi[7], E.B. Shields[28,p], Y. Shimizu[13], E. Shmanin[41], R. Shorkin[41], J.D. Shupperd[66], R. Silva Coutinho[66], G. Simi[30,q], S. Simone[21,h], N. Skidmore[54], T. Skwarnicki[66], M.W. Slater[51], J.C. Smallwood[61], E. Smith[62], K. Smith[65], M. Smith[59], A. Snoch[35], L. Soares Lavra[56], M.D. Sokoloff[63], F.J.P. Soler[57], A. Solomin[41,52], A. Solovev[41], I. Solovyev[41], R. Song[1], Y. Song[47], Y. Song[4], Y. S. Song[6], F.L. Souza De Almeida[66], B. Souza De Paula[3], E. Spadaro Norella[27,o], E. Spedicato[22], J.G. Speer[17], E. Spiridenkov[41], P. Spradlin[57], V. Sriskaran[46], F. Stagni[46], M. Stahl[46], S. Stahl[46], S. Stanislaus[61], E.N. Stein[46], O. Steinkamp[48], O. Stenyakin[41], H. Stevens[17],

JHEP07(2024)101

D. Strekalina[41], Y. Su[7], F. Suljik[61], J. Sun[29], L. Sun[71], Y. Sun[64], W. Sutcliffe[48], P.N. Swallow[51], F. Swystun[53], A. Szabelski[39], T. Szumlak[37], Y. Tan[4], S. Taneja[60], M.D. Tat[61], A. Terentev[48], F. Terzuoli[32,w], F. Teubert[46], E. Thomas[46], D.J.D. Thompson[51], H. Tilquin[59], V. Tisserand[11], S. T'Jampens[10], M. Tobin[5], L. Tomassetti[23,l], G. Tonani[27,o,46], X. Tong[6], D. Torres Machado[2], L. Toscano[17], D.Y. Tou[4], C. Trippl[42], G. Tuci[19], N. Tuning[35], L.H. Uecker[19], A. Ukleja[37], D.J. Unverzagt[19], E. Ursov[41], A. Usachov[36], A. Ustyuzhanin[41], U. Uwer[19], V. Vagnoni[22], A. Valassi[46], G. Valenti[22], N. Valls Canudas[42], H. Van Hecke[65], E. van Herwijnen[59], C.B. Van Hulse[44,y], R. Van Laak[47], M. van Veghel[35], R. Vazquez Gomez[43], P. Vazquez Regueiro[44], C. Vázquez Sierra[44], S. Vecchi[23], J.J. Velthuis[52], M. Veltri[24,x], A. Venkateswaran[47], M. Vesterinen[54], M. Vieites Diaz[46], X. Vilasis-Cardona[42], E. Vilella Figueras[58], A. Villa[22], P. Vincent[15], F.C. Volle[51], D. vom Bruch[12], V. Vorobyev[41], N. Voropaev[41], K. Vos[76], G. Vouters[10], C. Vrahas[56], J. Wagner[17], J. Walsh[32], E.J. Walton[1,54], G. Wan[6], C. Wang[19], G. Wang[8], J. Wang[6], J. Wang[5], J. Wang[4], J. Wang[71], M. Wang[27], N. W. Wang[7], R. Wang[52], X. Wang[69], X. W. Wang[59], Y. Wang[8], Z. Wang[13], Z. Wang[4], Z. Wang[27], J.A. Ward[54,1], M. Waterlaat[46], N.K. Watson[51], D. Websdale[59], Y. Wei[6], B.D.C. Westhenry[52], D.J. White[60], M. Whitehead[57], A.R. Wiederhold[54], D. Wiedner[17], G. Wilkinson[61], M.K. Wilkinson[63], M. Williams[62], M.R.J. Williams[56], R. Williams[53], F.F. Wilson[55], W. Wislicki[39], M. Witek[38], L. Witola[19], C.P. Wong[65], G. Wormser[13], S.A. Wotton[53], H. Wu[66], J. Wu[8], X. Wu[71], Y. Wu[6], K. Wyllie[46], S. Xian[69], Z. Xiang[5], Y. Xie[8], A. Xu[32], J. Xu[7], L. Xu[4], L. Xu[4], M. Xu[54], Z. Xu[11], Z. Xu[7], Z. Xu[5], D. Yang[4], S. Yang[7], X. Yang[6], Y. Yang[26,n], Z. Yang[6], Z. Yang[64], V. Yeroshenko[13], H. Yeung[60], H. Yin[8], C. Y. Yu[6], J. Yu[68], X. Yuan[5], E. Zaffaroni[47], M. Zavertyaev[18], M. Zdybal[38], M. Zeng[4], C. Zhang[6], D. Zhang[8], J. Zhang[7], L. Zhang[4], S. Zhang[68], S. Zhang[6], Y. Zhang[6], Y. Z. Zhang[4], Y. Zhao[19], A. Zharkova[41], A. Zhelezov[19], X. Z. Zheng[4], Y. Zheng[7], T. Zhou[6], X. Zhou[8], Y. Zhou[7], V. Zhovkovska[54], L. Z. Zhu[7], X. Zhu[4], X. Zhu[8], V. Zhukov[16], J. Zhuo[45], Q. Zou[5,7], D. Zuliani[30,q], G. Zunica[47]

[1] *School of Physics and Astronomy, Monash University, Melbourne, Australia*
[2] *Centro Brasileiro de Pesquisas Físicas (CBPF), Rio de Janeiro, Brazil*
[3] *Universidade Federal do Rio de Janeiro (UFRJ), Rio de Janeiro, Brazil*
[4] *Center for High Energy Physics, Tsinghua University, Beijing, China*
[5] *Institute Of High Energy Physics (IHEP), Beijing, China*
[6] *School of Physics State Key Laboratory of Nuclear Physics and Technology, Peking University, Beijing, China*
[7] *University of Chinese Academy of Sciences, Beijing, China*
[8] *Institute of Particle Physics, Central China Normal University, Wuhan, Hubei, China*
[9] *Consejo Nacional de Rectores (CONARE), San Jose, Costa Rica*
[10] *Université Savoie Mont Blanc, CNRS, IN2P3-LAPP, Annecy, France*
[11] *Université Clermont Auvergne, CNRS/IN2P3, LPC, Clermont-Ferrand, France*
[12] *Aix Marseille Univ, CNRS/IN2P3, CPPM, Marseille, France*
[13] *Université Paris-Saclay, CNRS/IN2P3, IJCLab, Orsay, France*
[14] *Laboratoire Leprince-Ringuet, CNRS/IN2P3, Ecole Polytechnique, Institut Polytechnique de Paris, Palaiseau, France*
[15] *LPNHE, Sorbonne Université, Paris Diderot Sorbonne Paris Cité, CNRS/IN2P3, Paris, France*
[16] *I. Physikalisches Institut, RWTH Aachen University, Aachen, Germany*

[17] Fakultät Physik, Technische Universität Dortmund, Dortmund, Germany
[18] Max-Planck-Institut für Kernphysik (MPIK), Heidelberg, Germany
[19] Physikalisches Institut, Ruprecht-Karls-Universität Heidelberg, Heidelberg, Germany
[20] School of Physics, University College Dublin, Dublin, Ireland
[21] INFN Sezione di Bari, Bari, Italy
[22] INFN Sezione di Bologna, Bologna, Italy
[23] INFN Sezione di Ferrara, Ferrara, Italy
[24] INFN Sezione di Firenze, Firenze, Italy
[25] INFN Laboratori Nazionali di Frascati, Frascati, Italy
[26] INFN Sezione di Genova, Genova, Italy
[27] INFN Sezione di Milano, Milano, Italy
[28] INFN Sezione di Milano-Bicocca, Milano, Italy
[29] INFN Sezione di Cagliari, Monserrato, Italy
[30] INFN Sezione di Padova, Padova, Italy
[31] INFN Sezione di Perugia, Perugia, Italy
[32] INFN Sezione di Pisa, Pisa, Italy
[33] INFN Sezione di Roma La Sapienza, Roma, Italy
[34] INFN Sezione di Roma Tor Vergata, Roma, Italy
[35] Nikhef National Institute for Subatomic Physics, Amsterdam, Netherlands
[36] Nikhef National Institute for Subatomic Physics and VU University Amsterdam, Amsterdam, Netherlands
[37] AGH — University of Krakow, Faculty of Physics and Applied Computer Science, Kraków, Poland
[38] Henryk Niewodniczanski Institute of Nuclear Physics Polish Academy of Sciences, Kraków, Poland
[39] National Center for Nuclear Research (NCBJ), Warsaw, Poland
[40] Horia Hulubei National Institute of Physics and Nuclear Engineering, Bucharest-Magurele, Romania
[41] Affiliated with an institute covered by a cooperation agreement with CERN
[42] DS4DS, La Salle, Universitat Ramon Llull, Barcelona, Spain
[43] ICCUB, Universitat de Barcelona, Barcelona, Spain
[44] Instituto Galego de Física de Altas Enerxías (IGFAE), Universidade de Santiago de Compostela, Santiago de Compostela, Spain
[45] Instituto de Fisica Corpuscular, Centro Mixto Universidad de Valencia — CSIC, Valencia, Spain
[46] European Organization for Nuclear Research (CERN), Geneva, Switzerland
[47] Institute of Physics, Ecole Polytechnique Fédérale de Lausanne (EPFL), Lausanne, Switzerland
[48] Physik-Institut, Universität Zürich, Zürich, Switzerland
[49] NSC Kharkiv Institute of Physics and Technology (NSC KIPT), Kharkiv, Ukraine
[50] Institute for Nuclear Research of the National Academy of Sciences (KINR), Kyiv, Ukraine
[51] University of Birmingham, Birmingham, United Kingdom
[52] H.H. Wills Physics Laboratory, University of Bristol, Bristol, United Kingdom
[53] Cavendish Laboratory, University of Cambridge, Cambridge, United Kingdom
[54] Department of Physics, University of Warwick, Coventry, United Kingdom
[55] STFC Rutherford Appleton Laboratory, Didcot, United Kingdom
[56] School of Physics and Astronomy, University of Edinburgh, Edinburgh, United Kingdom
[57] School of Physics and Astronomy, University of Glasgow, Glasgow, United Kingdom
[58] Oliver Lodge Laboratory, University of Liverpool, Liverpool, United Kingdom
[59] Imperial College London, London, United Kingdom
[60] Department of Physics and Astronomy, University of Manchester, Manchester, United Kingdom
[61] Department of Physics, University of Oxford, Oxford, United Kingdom
[62] Massachusetts Institute of Technology, Cambridge, MA, United States
[63] University of Cincinnati, Cincinnati, OH, United States
[64] University of Maryland, College Park, MD, United States
[65] Los Alamos National Laboratory (LANL), Los Alamos, NM, United States
[66] Syracuse University, Syracuse, NY, United States
[67] Pontifícia Universidade Católica do Rio de Janeiro (PUC-Rio), Rio de Janeiro, Brazil, associated to [3]
[68] School of Physics and Electronics, Hunan University, Changsha City, China, associated to [8]

[69] *Guangdong Provincial Key Laboratory of Nuclear Science, Guangdong-Hong Kong Joint Laboratory of Quantum Matter, Institute of Quantum Matter, South China Normal University, Guangzhou, China, associated to* [4]
[70] *Lanzhou University, Lanzhou, China, associated to* [5]
[71] *School of Physics and Technology, Wuhan University, Wuhan, China, associated to* [4]
[72] *Departamento de Fisica, Universidad Nacional de Colombia, Bogota, Colombia, associated to* [15]
[73] *Universität Bonn — Helmholtz-Institut für Strahlen und Kernphysik, Bonn, Germany, associated to* [19]
[74] *Eotvos Lorand University, Budapest, Hungary, associated to* [46]
[75] *Van Swinderen Institute, University of Groningen, Groningen, Netherlands, associated to* [35]
[76] *Universiteit Maastricht, Maastricht, Netherlands, associated to* [35]
[77] *Tadeusz Kosciuszko Cracow University of Technology, Cracow, Poland, associated to* [38]
[78] *Universidade da Coruña, A Coruna, Spain, associated to* [42]
[79] *Department of Physics and Astronomy, Uppsala University, Uppsala, Sweden, associated to* [57]
[80] *University of Michigan, Ann Arbor, MI, United States, associated to* [66]
[81] *Departement de Physique Nucleaire (SPhN), Gif-Sur-Yvette, France*

[a] *Universidade de Brasília, Brasília, Brazil*
[b] *Centro Federal de Educacão Tecnológica Celso Suckow da Fonseca, Rio De Janeiro, Brazil*
[c] *Hangzhou Institute for Advanced Study, UCAS, Hangzhou, China*
[d] *School of Physics and Electronics, Henan University, Kaifeng, China*
[e] *LIP6, Sorbonne Universite, Paris, France*
[f] *Excellence Cluster ORIGINS, Munich, Germany*
[g] *Universidad Nacional Autónoma de Honduras, Tegucigalpa, Honduras*
[h] *Università di Bari, Bari, Italy*
[i] *Universita degli studi di Bergamo, Bergamo, Italy*
[j] *Università di Bologna, Bologna, Italy*
[k] *Università di Cagliari, Cagliari, Italy*
[l] *Università di Ferrara, Ferrara, Italy*
[m] *Università di Firenze, Firenze, Italy*
[n] *Università di Genova, Genova, Italy*
[o] *Università degli Studi di Milano, Milano, Italy*
[p] *Università di Milano Bicocca, Milano, Italy*
[q] *Università di Padova, Padova, Italy*
[r] *Università di Perugia, Perugia, Italy*
[s] *Scuola Normale Superiore, Pisa, Italy*
[t] *Università di Pisa, Pisa, Italy*
[u] *Università della Basilicata, Potenza, Italy*
[v] *Università di Roma Tor Vergata, Roma, Italy*
[w] *Università di Siena, Siena, Italy*
[x] *Università di Urbino, Urbino, Italy*
[y] *Universidad de Alcalá, Alcalá de Henares, Spain*
[z] *Department of Physics/Division of Particle Physics, Lund, Sweden*
[†] *Deceased*

JHEP07(2024)101